New insights into marine-based paleo-ice sheet dynamics and glaciomarine depositional environment in an interfan area between ice stream-derived Trough Mouth Fans, Off West Svalbard

Akash Trivedi[1], Sudipta Sarkar[1], Stephan Ker[2], Timothy A Minshull[3], and Haflidi Haflidason[4,5]

[1]Department of Earth and Climate Science, Indian Institute of Science Education and Research Pune
[2]UMR 6538 Geo-Ocean
[3]School of Ocean and Earth Science, University of Southampton
[4]Department of Earth Science, University of Bergen
[5]Bjerknes Centre for Climate Research

September 09, 2024

Abstract

Highlights * We refined the seismic stratigraphic framework for the upper continental slope interfan region between the Kongsfjorden and Isfjorden Trough Mouth Fans.

Hosted file

Supplementary_Information_Trivedi_etal.docx available at https://authorea.com/users/829221/articles/1223283-new-insights-into-marine-based-paleo-ice-sheet-dynamics-and-glaciomarine-depositional-environment-in-an-interfan-area-between-ice-stream-derived-trough-mouth-fans-off-west-svalbard

New insights into marine-based paleo-ice sheet dynamics and glaciomarine depositional environment in an interfan area between ice stream-derived Trough Mouth Fans, Off West Svalbard

Akash Trivedi[1*], Sudipta Sarkar[1], Stephan Ker[2], Timothy A. Minshull[3], Haflidi Haflidason[4]

Affiliations:

[1]Department of Earth and Climate Science, Indian Institute of Science Education and Research Pune, Pune, 411008, India

[2] Ifremer, UMR 6538 Geo-Ocean, F-29280 Plouzané, France

[3]School of Ocean and Earth Science, University of Southampton, Waterfront Campus, European Way, Southampton SO14 3ZH, UK

[4] Department of Earth Science, University of Bergen, Box 7803, N-5020 Bergen, Norway and Bjerknes Centre for Climate Research, N-5007 Bergen, Norway

*Correspondence to: Akash Trivedi (trivedi.akash@students.iiserpune.ac.in)

Highlights

- We refined the seismic stratigraphic framework for the upper continental slope interfan region between the Kongsfjorden and Isfjorden Trough Mouth Fans.
- The study identifies distinct Weichselian shelf edge glaciations, providing a detailed characterization of glacial units, including calving episodes and debris flows.
- A debris flow simulation is presented to elucidate the underlying mechanisms governing the observed debris morphology.

Abstract: Understanding the dynamic history of the marine-based paleo-Svalbard Ice Sheet is crucial, as it provides insights into past climate change and the interactions between the ocean system and the cryosphere. High-resolution seismic imaging is essential for deciphering the glacial history of the western Svalbard continental margin, which has experienced multiple glaciations throughout the Quaternary period. Glaciomarine sediments preserved in the continental margins provide a detailed record of these events. This study integrates high-resolution air gun seismic (vertical resolution 5 m), and deep-towed seismic data (vertical and horizontal resolutions 1 and 3 m, respectively) along with age constraints to refine the seismic stratigraphic framework, depositional architecture, and sedimentation processes of the interfan area between the Kongsfjorden and Isfjorden Trough Mouth Fans (TMFs). New age constraints indicate that the build-up of the Kongsfjorden TMF began around 1.2 million years ago. Our data analysis reveals four distinct shelf-edge glaciations during the Weichselian period (120–110 ka, ~90 ka, 61–54 ka, and ~24 ka). These glacial

units on the upper continental slope contain debris materials transported by slow-moving ice sheets. During maximum glacial expansion, iceberg calving created V-shaped indentations, and glaciogenic debris flows carved erosional troughs. Seismic interpretation and debris flow modeling aided in understanding the development of lensoid debris morphology, stacking patterns, and the evolution of debris lobes resulting from local variations in bottom topography. This study underscores the significance of using multiple high-resolution seismic data sources to enhance our understanding of the glacial history and depositional processes in the interfan region.

1. Introduction:

A detailed record of past glacial activity and the dynamic history of the ice sheet are crucial for understanding climate change, predicting the fate of ice sheets, and forecasting future environmental changes, such as assessing the stability of present-day ice sheets in response to climate warming. Glaciomarine sediments found in polar continental margins serve as invaluable records of past glacial activity. These sedimentary archives provide insights into stratigraphic evolution, spatiotemporal patterns of glacial erosion, and the history of ice sheet advancements and retreats (Vorren & Laberg, 1997; Ó Cofaigh et al., 2003). The spatial variability in sedimentation styles along glaciated continental margins reflects the dynamics of ice sheets across polar regions. For example, in the Arctic Archipelago of Svalbard, fan-shaped bathymetric features known as trough-mouth fans (TMFs) on the continental slope represent basinward-prograding sequences of glacial debris flows (Fig. 1a). They resulted from the high sediment supply by fast-flowing paleo-ice streams at the shelf break. In contrast to TMFs, slow-moving ice covered the shelf region between the paleo-ice streams.

The continental shelf of Svalbard experienced recurrent cycles of glacial waxing and waning during the Pliocene and Pleistocene epochs, resulting in significant changes in sedimentation and erosion patterns (Solheim et al., 1998; Butt et al., 2000). The records of glaciations and deglaciations onshore and on the shelf are affected by glacial erosion, complicating the reconstruction of glacial-deglacial cycles. TMFs offer well-preserved depositional records that provide insights into ice sheet activity. The glacial history of Svalbard is deciphered from seismic stratigraphic analysis and age models determined from boreholes. For example, Ocean Drilling Program (ODP) Sites 910, 911 (Leg 151, Myhre et al., 1995) in the Yermak Plateau provide stratigraphic details of northern Svalbard, while ODP Site 986 between Belsund and Isfjorden TMFs provide age constraints on the glacial development of western Svalbard (Fig. 1a, Leg 162, Forsberg et al., 1999). Laberg and Vorren (1996) and Hjelstuen et al. (1996) established the initial framework for the Bear Island TMF and Storfjorden TMF, respectively, and Vorren et al. (1991), Faleide et al. (1996), and Ryseth et al. (2003) reconstructed the glacial history of the western and southwestern Barents Sea. Additionally, Geissler and Jokat (2004), Sarkar et al. (2011), and Mattingsdal et al. (2014) developed more detailed stratigraphic constraints on glacial history of the northern and northwestern Svalbard margins. Building on this foundation, Alexandropoulou et al. (2021) provided a comprehensive seismic stratigraphic framework spanning the past 2.7 million years for the Barents Sea and western Svalbard. The Pliocene-Pleistocene glacial history of Svalbard is characterized by distinct phases of ice sheet development, e.g., an initial growth period from 2.7 to 1.6 Ma, followed by an expansion phase from 1.5 to 0.42 Ma, and extensive, dynamic glaciations across the Barents Sea resulting in high sedimentation after ~0.42 Ma (Alexandropoulou et al., 2021).

Although there is a comprehensive understanding of the stratigraphic development of the TMFs, our knowledge of the interfan glacial history remains limited and inadequate. This leaves significant gaps in our ability to reconstruct glacial processes in these regions, such as the interfan region between the Kongsfjorden and Isfjorden TMFs. The interfan region has also garnered significant attention due to ongoing methane seeps caused by methane hydrate dissociation in highly heterogeneous glaciogenic sediments (Westbrook et al., 2009; Sarkar et al., 2012), necessitating a detailed characterization of the strata. Previous attempts to understand the westward expansion of the Svalbard ice sheet were made by Sarkar et al. (2011) for the Kongsfjorden TMF region and Solheim et al. (1998) for the Isfjorden TMF region. Moreover, the Kongsfjorden region experienced multiple episodes of shelf-edge glaciations, including an initial paleo-ice stream development sometime between ~0.99 and 1.5 Ma (Sarkar et al., 2011). However, due to the unavailability of precise age markers, it is difficult to constrain the exact timing of Kongsfjorden TMF development.

In the regional stratigraphic framework, the Weichselian stratigraphic development is less clear, mainly due to inadequate age controls, creating a gap in our understanding. Although there is a consensus that multiple shelf-edge glacial advances occurred during the Weichselian, uncertainties exist regarding the exact number and timing of these advances. Onshore coastal records suggest that during the last glacial stage (118–11.6 ka), shelf-edge glaciations off the western Svalbard continental margin occurred at least three times, reaching its maximum extent around 118–108 ka, 75–50 ka, and 32–20.5 ka (Mangerud et al., 1998). This observation suggests that the glacial maximum during Marine Isotope Stage (MIS) 4 (75–50 ka) lasted approximately twice as long as both MIS 5d (118–108 ka) and the Last Glacial Maximum (LGM), with each spanning approximately 10,000 years. Based on work in the Kongsfjorden area, Eccleshall et al. (2016) suggested that the ice sheet expanded to the shelf break during MIS 5b (93–83 ka) but not during MIS 4 (75–50 ka). Finally, Alexanderson et al. (2018) suggested a highly fluctuating Svalbard ice sheet configuration during the Weichselian, with five advances peaking at around 110, 90, 70, 45 and 25 ka.

To refine the reconstruction of the Weichselian glacial history and distinguish between the conflicting ideas listed above, high-resolution seismic data capable of accurately resolving stratigraphic units are required, coupled with improved age controls. Wiberg et al. (2022) identified three glacial advances at 90 ka, 75–54 ka, 38–24 ka using high-resolution TOPAS sub-bottom profiler data and ages from a sediment core collected from the Kongsfjorden TMF region. However, the knowledge of glacial evolution and depositional processes across the glaciated continental shelf and the upper continental slope in the interfan area between the Kongsfjorden TMF and Isfjorden TMF, west of Prins Karls Forland (**Figs. 1a and 1b**) is still lacking due to limited high-resolution seismic surveys.

This study aims to refine the seismic stratigraphic framework of the interfan region situated between the Kongsfjorden and Isfjorden cross-shelf troughs, with a particular emphasis on delineating the transition to the Mid-Pleistocene glacial advance. Additionally, we seek to establish the Weichselian seismic stratigraphic framework of the interfan area by integrating an improved age model with seismic interpretation derived from high-resolution two-dimensional (2D) seismic data. Finally, we aim to improve the understanding of the glaciomarine sedimentary environment and depositional processes occurring at the continental slope within the interfan region.

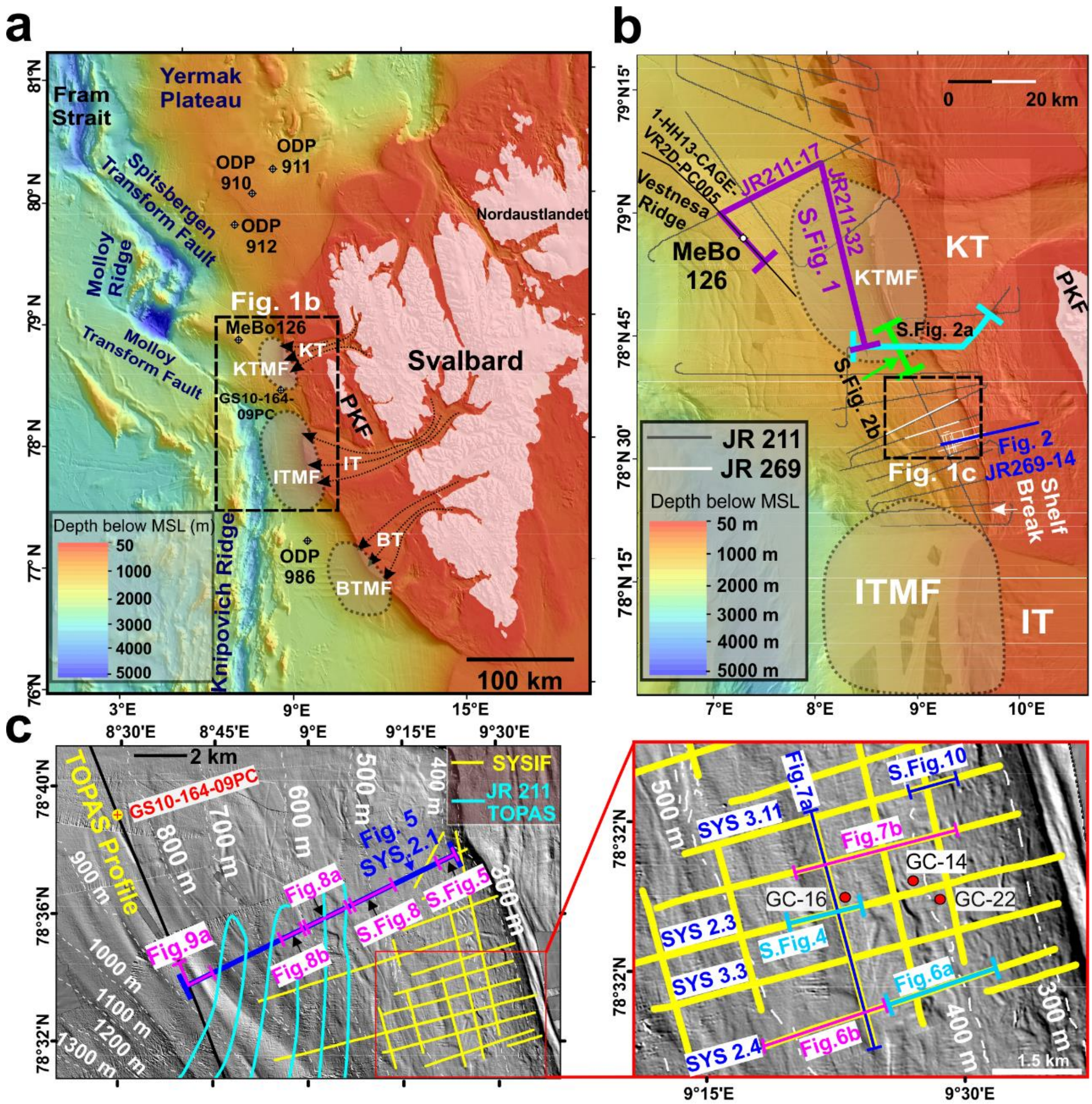

Figure 1. Study area map showing the location of 2D air gun seismic and SYSIF lines. (a) The bathymetry image shows the mid-oceanic ridge and transform fault system west off Svalbard, boreholes on the Yermak Plateau, and western Svalbard. Glacial cross-shelf troughs (Kongsfjorden Trough (KT), Isfjorden Trough (IT), Belsund Trough (BT) and respective trough mouth Fans (TMFs) were formed by paleo-ice streams. PKF is Prins Karls Forland, (b) 2D seismic lines from the JR211 and JR269A cruises. The bathymetry is a compilation of multiple cruises, such as JR211 and surveys conducted by the Norwegian Hydrographic Survey (Sarkar et al., 2012) (**Suppl. Table 1**), (c) SYSIF seismic lines and TOPAS sub-bottom profiler lines used to develop the seismic stratigraphic framework in the interfan region. The enlarged inset displays the locations of gravity cores collected during the MSM57 cruise in August 2016 aboard the RV Maria S. Merian (Bohrmann et al., 2017).

2. Study Area: geological background and brief glacial history

During the Early Eocene, Svalbard began separating from northeast Greenland as a result of right lateral strike-slip movement along the West Spitsbergen shear zone. The strike-slip movement was followed by a transpressive deformation phase that is referred to as the West Svalbard Orogeny, resulting in the formation of a foreland fold-and-thrust belt (Harland et al., 1997). The western Spitsbergen thrust belt encompasses the Prins Karls Forland (PKF, Fig. 1a) and the western Svalbard coast. The Forlandsundet Graben separates the Svalbard west coast from the Prins Karls Forland (Ritzmann et al., 2004).

During the Middle Eocene to Early Oligocene, a shift from transpression to transtension instigated oblique extension. Seafloor spreading connecting the Arctic Gakkel Ridge with the Mohns and Knipovich Ridges led to the opening of the Fram Strait oceanographic gateway, allowing communication between the North Atlantic and the Arctic Ocean (Ritzmann & Jokat, 2003). During the Neogene, westward flowing paleo-ice streams released large masses of glacial sediments, called Trough Mouth Fans (TMFs), in front of cross-shelf troughs (Fig. 1a). These TMFs left distinct geomorphic features on the slope bathymetry, appearing as bathymetric bulges in front of the cross-shelf troughs (**Fig. 1a**). The TMFs are mainly built by stacked glacial debris flow lobes (Laberg and Vorren, 1995; Hjelstuen et al., 1996).

The onset of the Sjubrebanken TMF development provides evidence of the first shelf-edge glaciations in northwestern Svalbard around 2.58 Ma (Sarkar et al., 2011; Alexandropoulou et al., 2021) as a result of early Northern Hemispheric Glaciation (Jansen and Sjøholm, 1991; Mudelsee and Raymo, 2005), although glaciers did not reach the western Svalbard shelf break during that time (Sarkar et al., 2011; Mattingsdal et al., 2014). The presence of the ice-rafted debris from ODP site 986 (located between the Bellsund TMF and Isfjorden TMF) post 1.6 Ma indicates shelf-edge glaciations in western Svalbard after that time (Butt et al., 2000). During 1.5–1.2 Ma, glaciers covered a wider Svalbard and Barents Sea region (Alexandropoulou et al., 2021). A prominent and extensive glacial expansion occurred in the Svalbard and Barents Sea regions ~1.0 to 0.94 Ma, corresponding to a global increase in ice volume, during the Mid-Pleistocene revolution (Hjelstuen et al., 2007; Mudelsee and Stattegger, 1997). The incision of the Kongsfjorden cross-shelf trough (KT, Fig. 1b), initiated sometime between 0.99 and 1.5 Ma by ice stream activity, lead to the formation of the Kongsfjorden TMF (Sarkar et al., 2011).

3. Data and Methods

3.1. Multichannel seismic reflection data

Multichannel seismic reflection (MCS) data were collected on the shelf and slope of the interfan area (Fig. 1b) during cruise JR269A in 2011. The seismic survey employed a 60-m streamer with sixty 1-m hydrophone groups. The seismic source was a 1.46 l GI air gun comprising a 0.73 l-generator and a 0.73 l-injector. The air gun was towed at 1.5 m depth and operated in harmonic mode at a nominal pressure of 140 bar (2000 psi). The shot interval was maintained at 6 s, corresponding to 12 m shot spacing. The duration of the recording of seismic trace was 3 s, with a sampling rate of 0.5 ms.

The processing steps of MCS data involved (i) merging marine geometry to the raw shots, (ii) common midpoint (CMP) sorting with the spacing between individual CMP bins at 2 m, (iii) Ormsby bandpass filtering that is characterized by specific corner frequencies set at 10 Hz, 30 Hz, 600 Hz, and 1000 Hz; (iv) normal move-out correction, (v) stacking and (vi) post-stack migration (Stolt f-k). Apart from the seismic lines from the JR269A cruise, this study includes 2D MCS lines obtained during the JR211 cruise (Sarkar et al., 2011). These lines were collected using a 96-channel streamer with an active length of 600 m and a GI air gun with a volume of 2.45 l.

3.2. High-resolution SYSIF Data

During cruise JR269A in 2011, a total of 125 km of deep-towed SYSIF seismic lines (Fig. 1c) were acquired from the upper continental slope of the interfan region between the Isfjorden and Kongsfjorden TMFs in water depths ranging from 250 to 875 m (Ker et al., 2014). A Janus Helmholtz transducer was used as the SYSIF seismic source, which transmitted a chirp signal in the high-frequency bandwidth (220–1050 Hz). The receiver was a single hydrophone with a 10 m offset from the source. The processing workflow of SYSIF data consists of i) performing a source signature deconvolution with the far-field recording at normal incidence to increase the vertical resolution (Ker et al., 2010), ii) applying a depth correction as the altitude of SYSIF is towed at a height of 100 m above the seabed, and iii) migration with a velocity of 1500 m/s. In the uppermost continental slope, the maximum penetration achieved by the SYSIF signal is approximately ~100 ms or ~75 m in glaciomarine deposits. The signal penetration is around 200 ms or ~150 m below the seabed in hemipelagic sediments on slopes. The horizontal resolution varies from 1 to 3 m depending on the depth of the reflectors that could be imaged in the subsurface. The dominant frequency peaked between 400–750 Hz, resulting in a vertical resolution of 0.5–1 m.

3.3 TOPAS sub-bottom profiler data

We utilized hull-mounted TOPAS sub-bottom profiler data acquired during two separate cruises: the JR211 expedition onboard the RRS James Clark Ross and another expedition led by the University of Bergen aboard the RV G.O. Sars. The TOPAS profiling during JR211 employed a parametric acoustic source. The vertical resolution of JR211 TOPAS data is 0.167 m based on a velocity assumption of 1500 m/s (Fang et al., 2016). During the cruise onboard RV G.O. Sars, the TOPAS PS18 parametric sub-bottom profiler system was used, providing TOPAS profiles with a vertical resolution of 0.3–0.35 m (Wiberg et al., 2022).

3.4 Previous and updated regional seismic-stratigraphic correlation

Sarkar et al. (2011) developed a seismic stratigraphic framework of the Kongsfjorden TMF and the interfan region between the Kongsfjorden and Isfjorden TMFs using six seismic horizons (A1–A6). However, their chronostratigraphic framework lacked comprehensive age controls for these horizons. To address this limitation, we established an updated seismic stratigraphy with improved age controls for both the Kongsfjorden TMF and the interfan region. This process involved tracing the regional seismic horizons (named X1, X2, R1-R4, R4A, and R5–R7) along a composite seismic line connecting the MeBo 126 drill site (Dessandier et al., 2021) to the Kongsfjorden TMF (**Suppl. Fig. 1)** and upper continental slope and the interfan region between Kongsfjorden and Isfjorden TMFs (**Fig. 1b**). **Suppl. Table 2** provides an overview of the regional seismic reflectors and their corresponding age constraints on the west Svalbard slope. The regional horizons R7, R4, and R2 could be traced from the continental slope to the outer shelf, but the tracing of other reflectors in the interfan slope and shelf is difficult due to poor reflection continuity.

3.5. Debris flow modeling

In this study, we employed Rapid Mass Movement Simulation (RAMMS) debris flow numerical modeling (Christen et al., 2010) to gain insights into the behaviour and runout characteristics of debris flows. Our aim was to simulate glacial debris flow dynamics, enabling us to correlate model-predicted results with seismic observations of debris flow. To constrain the debris flow model, we took into account the shape, dimensions (length along slope-perpendicular direction and thickness) of debris lobes, and runout distance from the shelf break, considering the release location as the edge of a submarine till-wedge.

RAMMS uses a depth-averaged shallow water equation based on the conservation of mass and momentum (Christen et al., 2010). In RAMMS, the Voellmy rheology model (Salm et al., 1990; Salm, 1993) was used to simulate debris flow behaviour by utilizing two key parameters: the Coulomb basal friction coefficient (μ) for solid-like behaviour and the viscous drag coefficient (ξ) for fluid-like behaviour. Additionally, including a yield stress (Bartelt et al., 2015) term addresses the cohesion observed in materials like muddy debris. The relationship between frictional resistance S (Pa), frictional coefficient, viscous drag coefficient, and yield stress is given by Equation (1).

$$S = \mu N + \frac{\rho g u^2}{\xi} + (1-\mu)N_0 + (1-\mu)N_0 e^{-\frac{N}{N_0}} \quad (1)$$

In this equation, N_0 (Pa) is the yield stress, ρ (kg/m^3) is the density, g (m/s^2) is the gravitational acceleration, and u (m/s) represents x- and y-components of velocity. The frictional coefficient μ represents Coulomb friction, and the coefficient ξ (m/s^2) represents turbulence friction parameters. N (Pa) represents the normal stress.

During the trial runs, the coefficients μ and ξ were varied, but they were kept constant throughout one simulation. The goal of debris flow modeling was to identify flow patterns for a predefined set of debris flow rheological properties, and we did not aim for an exhaustive treatment of all debris flow intricacies, such as debris flow transforming into turbidity currrent. Our simulations did not account for erosion and sediment entrainment models, focusing only on the cohesive behaviour of debris flow. Modeling parameters used in RAMMS are provided in **Suppl. Table 3**.

4. Results

The seismic stratigraphic description of the interfan shelf and slope regions is presented using the MCS profiles. These profiles, acquired with an airgun source, have limited resolution of the shallowest stratigraphy due to the long seabed wavelet, which obscures finer stratigraphic details. High-resolution SYSIF lines are used to improve the stratigraphic description of the top 70–100 m below the seabed on the slope.

4.1. Continental shelf stratigraphy of the Interfan area based on 2D MCS lines:

A prominent erosional unconformity identified as the Upper Regional Unconformity (URU) serves as the erosional base for a major glacial advance on the continental shelf, and it is correlated with the reflector R4A (**Fig. 2**) in the interfan region between the Kongsfjorden and Isfjorden TMFs. This correlation suggests that significant erosion, reaching the URU level, happened around 1.2 Ma (corresponding to the age of the R4A reflector, **Suppl. Table 2**). The URU dips westward at an angle of 0.3-0.9° in the outer shelf. The geological succession below the URU/R4A includes seismic units IU-5 and IU-6, while the overlying succession is represented by units IU-1 to IU-4 (**Fig. 2**).

The pre-URU stratigraphic units, IU-5 and IU-6, are separated by reflector C (Insets 1 and 2, **Fig. 2**) in the outer shelf. Unit IU-6 is nearly transparent with weak internal reflections, suggesting the presence of crystalline rocks, and the weak reflectivity is presumably due to the hard rocks. IU-5 is represented by stratified and westward-dipping reflection patterns (Inset 2, **Fig. 2**). The top of unit IU-5 is truncated by the erosional surface (URU). The transition from chaotic, transparent facies in IU-6 to stratified facies in IU-5 is inferred to represent a transition from crystalline basement to overlying sedimentary layers in the outer shelf region. In the upper slope, well-stratified reflections and upslope climbing waves are present in unit IU-5.

The geological succession overlying URU is represented by a stack of seaward-dipping wedge-shaped seismic units in the outer shelf. The post-URU geological succession is classified into four units: IU-4, delineated by R4A at the base and R4 at the top; IU-3, marked by R4 at the base and R2 at the top; IU-2, defined by R2 at the base and W at the top; and the topmost unit, IU-1, bounded by W at the base and the seabed at the top.

Unit IU-4 predominantly consists of wedge-shaped chaotic facies within the outer shelf region of the interfan area (**Fig. 2**). The thickness of wedge-shaped chaotic packages increases as they extend seaward. These chaotic reflections are interbedded with oblique westward dipping (3 to 6°) downlapping reflections, spanning ~2 km in the E-W direction. The reflector M on the outer shelf truncates the upper part of unit IU-4. The chaotic wedge facies is interpreted as a glaciogenic prograding wedge. The transparent and structureless nature suggests the presence of glaciogenic debris, while the moderate-amplitude continuous reflections indicate a transition from debris flow to the settling of hemipelagic sediments. In contrast to the interfan region, unit IU-4 demarcates the onset of glacial TMF development in the Kongsfjorden TMF region (**Suppl. Figs. 2a and 2b**).

Unit IU-3 reveals seaward-prograding clinoforms that extend from the outer shelf to the upper slope, with their top truncated by reflector M in the outer shelf and shelf break (**Fig. 2**).

Unit IU-2, in the shelf break and upper slope, consists of prograding clinoforms characterized by moderate-amplitude reflections separating chaotic regions. They extend basinward, gradually thinning downslope, and are interpreted as glaciogenic prograding sequences. Sarkar et al. (2011) observed and compared the extent of prograding wedge facies in the interfan area and in the Kongsfjorden TMF. They noted that the interfan region underwent moderate shelf progradation (~5-7 km), suggesting a depocenter fed by slow-moving ice sheets. In contrast, the Kongsfjorden TMF exhibited more extensive prograding packages, extending approximately 30 km in an E-W direction on the upper slope, indicating significant glaciogenic deposition from ice streams (Sarkar et al., 2011). The erosional reflector M in the outer shelf correlates with the slope reflector W in the slope. Reflector M diverges toward the basin from the URU.

Unit IU-1 shows prograding clinoforms at the shelf break and on the outer shelf (**Fig. 2**). In the outer shelf region, IU-1 displays high-amplitude, undulating reflections with some showing landward dipping (4.8–5°) segments (**Fig. 2**, Inset 1). They represent deposits affected by glacial tectonics, such as thrusting, that survived glacial erosion. Additionally, moraine complexes were deposited after the Last Glacial Maximum, marking periods of standstill during the ice sheet retreat.

On the upper continental slope (water depths 375–600 m), Units IU-1–4 display a complex intercalation of stratified contorted reflections interspersed with intermittently chaotic regions (**Fig. 2**). Additionally, erosional incisions are present in this region. For example, reflector W truncates regional reflector X1 in the upper slope region (Fig. 2).

The URU shows short-wavelength undulations, such as upward convex morphology, above the crystalline rocks (**Fig. 2**, Inset 2). Further westward, the URU is concave and truncates underlying well-stratified beds. There is a net glaciogenic sediment accumulation, shelf progradation, and aggradation basinward of the concave segment of the URU. The slope reflector R4A correlates with the URU, indicating that R4A represents a correlative conformity, marking the distal extension of the URU. The presence of gently seaward-

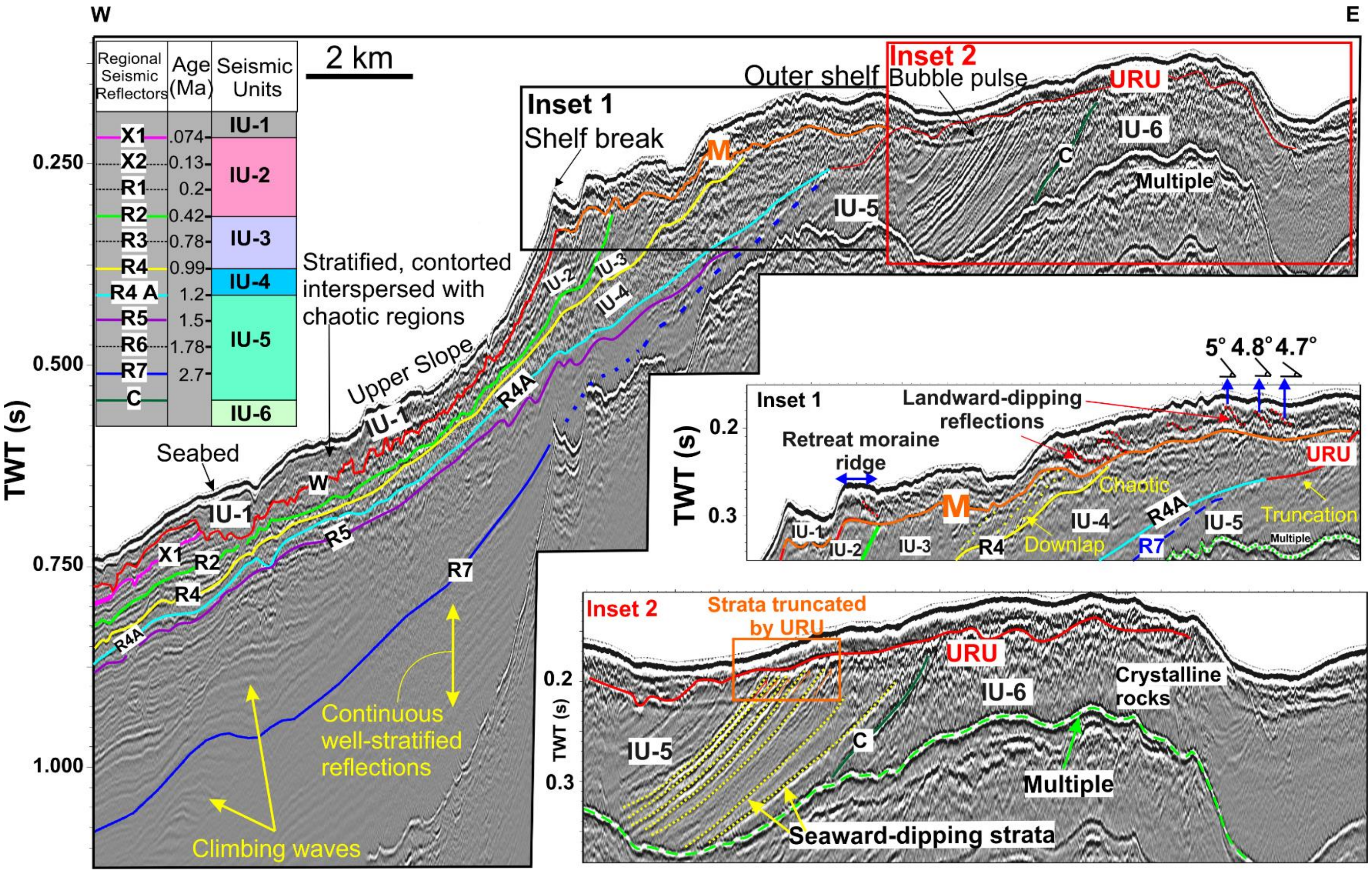

Figure 2. Seismic line JR269-14 showing the seismic units in the interfan area (location is shown in Fig. 1b). Seismic unit IU-6 in the shelf shows a nearly transparent region that likely represents crystalline rocks and IU-5 shows seaward-dipping strata. The Upper Regional Unconformity (URU) truncated the top of IU-5 and merged with the slope reflector R4A (Insets 1 and 2). Seismic units IU-4–IU-1 in the outer shelf region consist of westward-dipping oblique clinoforms. Moderate-amplitude reflections enclose chaotic, transparent, and incoherent reflections, indicating seaward progradation. Unit IU-1 shows deformed till with landward-dipping reflections on the outer shelf (Inset 1).

dipping sedimentary sequences below the URU and the curvature on the URU likely indicate erosion of softer sedimentary strata and westward subsidence about a convex hinge zone. Differential subsidence plays an important role in the accumulation of the sedimentary wedge along the margin. Several factors contribute to this subsidence, including compaction of sediments deposited before URU/R4A and glacial loading (Løtveit et al., 2019).

4.2. Slope stratigraphy of the Interfan area based on high-resolution SYSIF data

Here the seismic stratigraphy of the upper continental slope is established based on SYSIF seismic data. The seismic stratigraphy comprises a description of seismic facies in **Table 2**, followed by a description of the seismic units, their interpretation, and key bounding reflectors in **Table 3**. **Suppl. Fig. 3** serves as a bridge, integrating the air gun and SYSIF seismic units. The seismic stratigraphic framework is correlated with the established framework of Wiberg et al. (2022).

4.2.1. SYSIF Seismic facies

The seismic facies is broadly classified into two categories: stratified and chaotic facies. A stratified facies represents a set of parallel, continuous reflections, while a chaotic facies is dominated by incoherent, discontinuous reflections. The stratified facies is subdivided into three types, SF 1-3, and the chaotic facies is subdivided into 4 varieties, CF1-4 (**Table 2**).

4.2.2. Seismic unit description from the SYSIF data on the slope

Ten seismic reflectors (Seabed, S1-S5, S6A, S7, and S7A–B) divide the SYSIF seismic lines into 9 major seismic units: SU 1 (youngest) to SU 9 (oldest) (**Table 3**). The seismic facies and thickness variations of units SU 1–5 are shown in **Figs. 3 and 4**, respectively. The deeper seismic units (SU 6–9) are untraceable in the upper slope due to poor imaging and partly because of erosion; hence, facies maps and unit thickness maps for these units are not generated. The detailed characteristics and interpretations of each seismic unit are provided below.

Table 2. Seismic facies template based on SYSIF data for the interfan area.

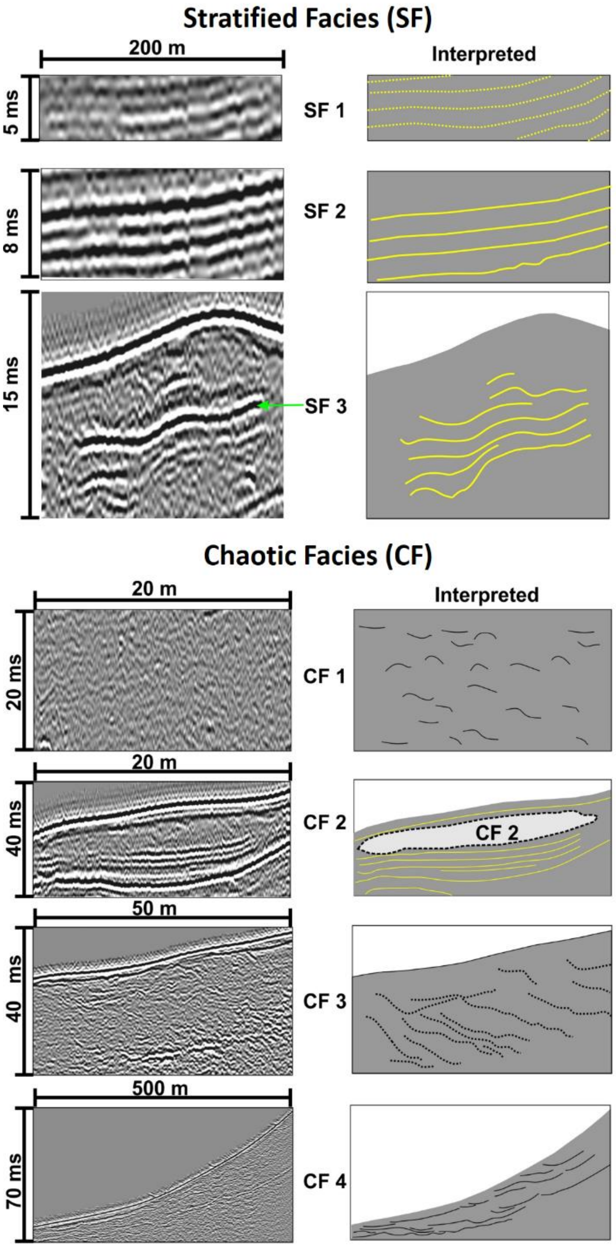

Description

SF 1: This facies is characterized by parallel to sub-parallel, low to medium amplitude reflections with a conformable top and bottom. The low amplitude indicates fine-grained deposits like plumite.

SF 2: This facies is similar to SF 1 but exhibits medium to high amplitude reflections. The high amplitude indicates coarser sediments such as sand.

SF 3: The facies is similar to SF 2 but exhibits semi-continuous, choppy, and isolated reflections (maximum length ~200m). They show interbedding with chaotic reflections. The medium-high amplitude reflects the deposition of coarser sediments and interpreted as isolated turbidite.

CF 1: This facies exhibits low-amplitude, discontinuous reflections that are nearly transparent and structureless. They fill paleo erosional surfaces. The facies represents glaciogenic debris flows filling pre-existing topographic lows.

CF 2: Similar to CF1 but have a lenticular/lensoid geometry. CF 2 deposits are structureless with an irregular erosional base, indicating their gravity-driven nature.

CF 3: Similar to CF 2 but has an overall rhombic geometry, and oblique depositional succession. The boundary between stacked lobes shows a moderate amplitude. This facies represents debris lobes resting on each other, indicating multiple local episodes of debris flow deposition.

CF 4: This facies exhibits a set of concave low to medium amplitude semi-continuous reflections. These packages represent bottom set of the S-shaped glaciogenic/prograding clinoform.

Table 3. SYSIF seismic units and their bounding reflectors in the interfan area.

SYSIF Seismic Units	Top reflector	Bottom reflector
SU 1	Seabed	S1
SU 2	S1	S2
SU 3	S1/S2	S3
SU 4	S3	S4
SU 5	S4	S5/ES-1
SU 6	S5	S6A
SU 7	S6A/ES-1	S7/ES-2
SU 8	S7/ES-2	S7A
SU 9	S7A	ES-3/S7B

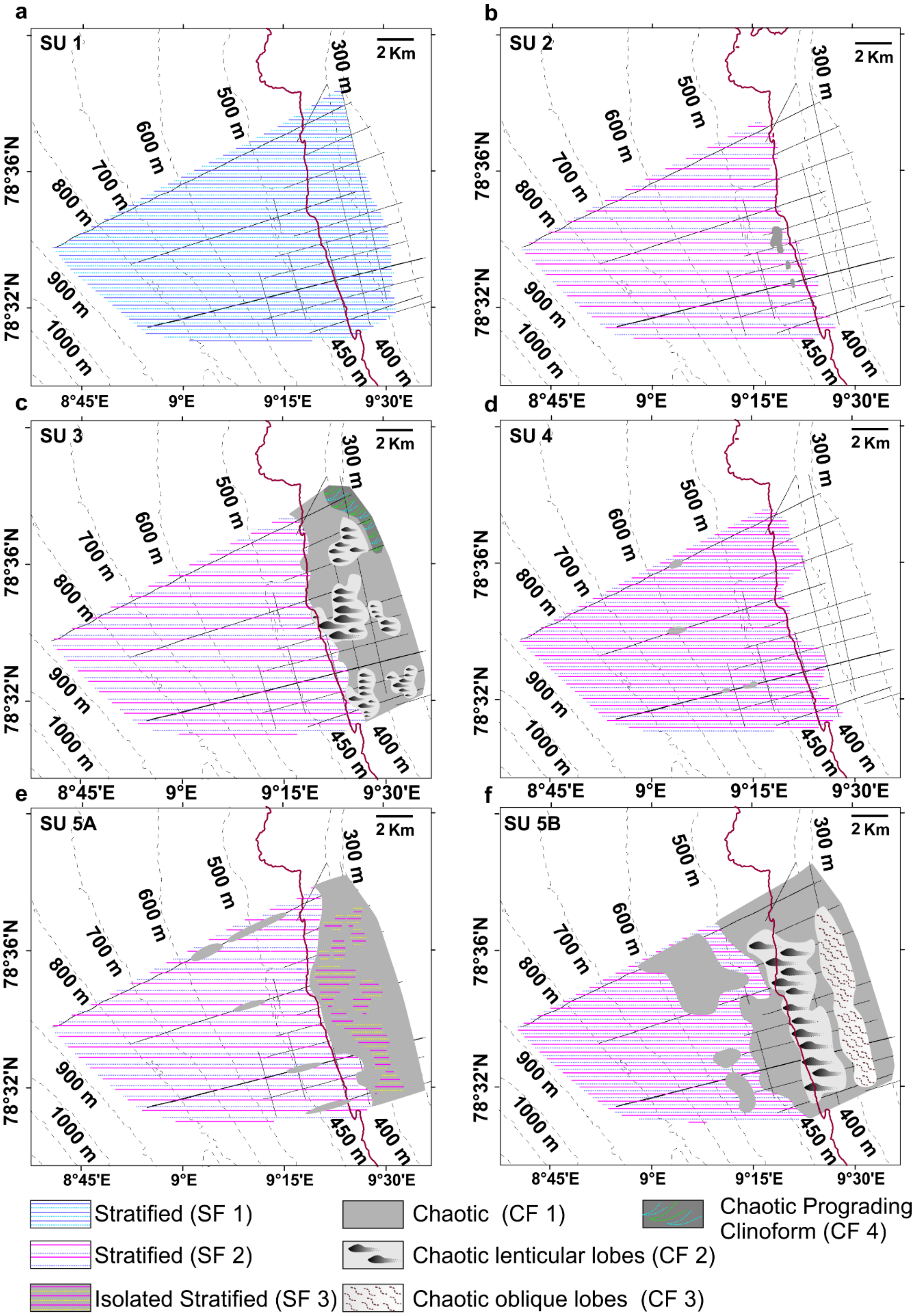

Figure 3. Spatial variation of different facies in stratigraphic units SU 1-5. The stratified facies (SF) are predominantly present >450 m except in SU 1, as it covers shallower depths up to 300 m. The chaotic facies in SU 3, SU 5A, and 5B indicate glaciogenic debris flows.

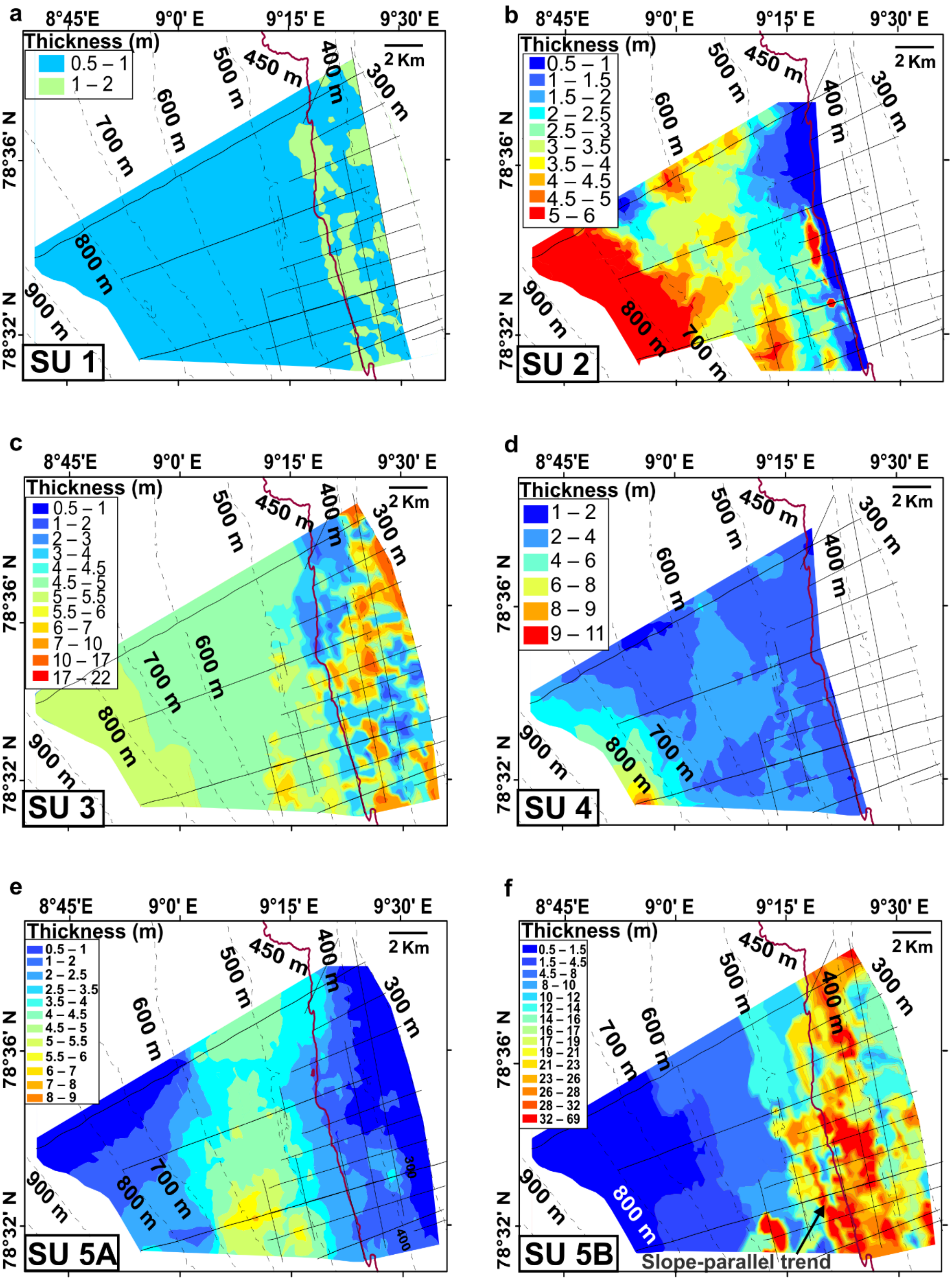

Figure 4. Map showing the thickness variations of stratigraphic units SU 1-5. Comparison of with Fig. 3 shows that the thickness of the CF-2 glaciogenic facies in SU 5B is much higher than in SU 3.

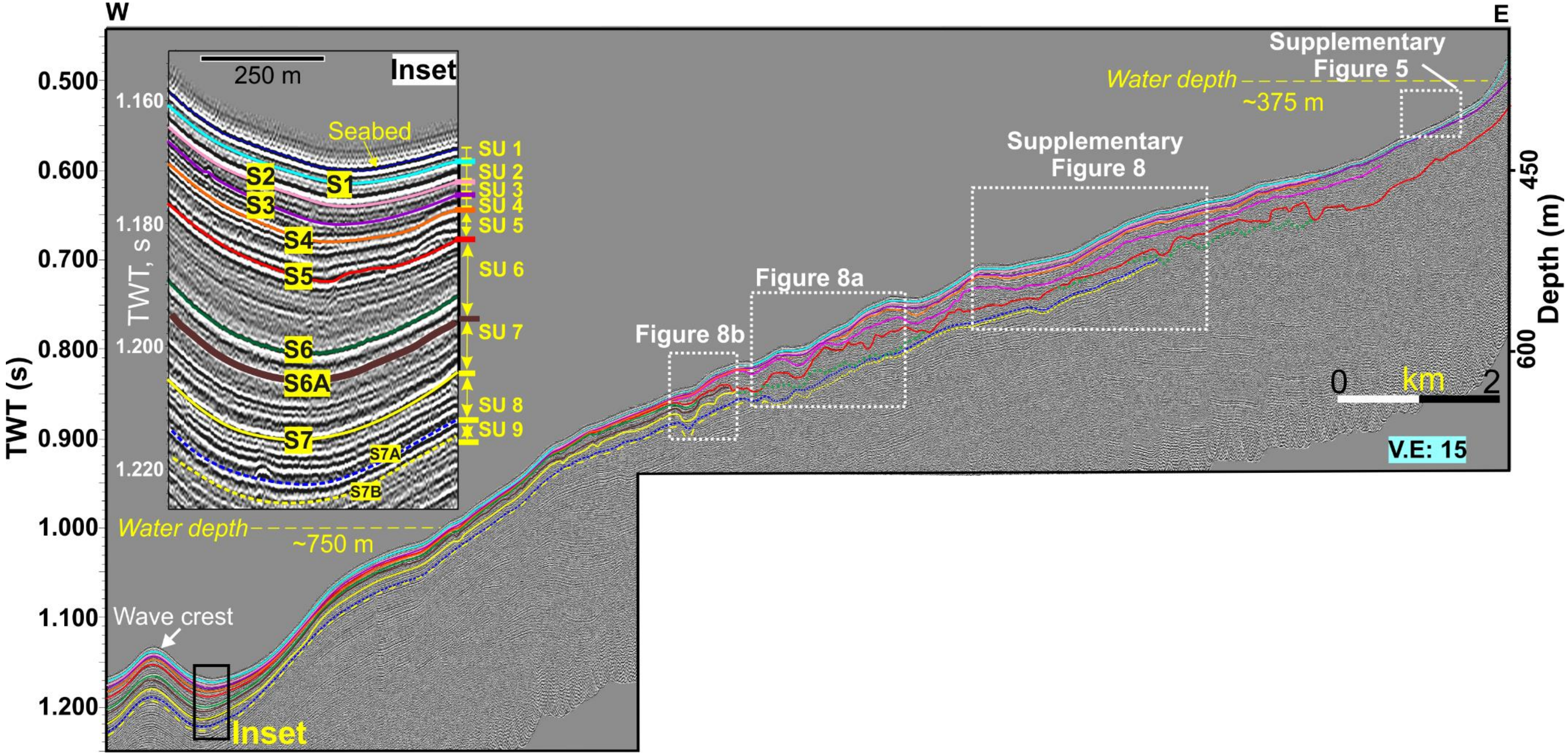

Figure 5. Slope-perpendicular SYSIF seismic profile 2.1 (location in Fig. 1c) showing key reflectors (Seabed, S1-S7, S7A-B) and seismic units in the interfan area. A sediment wave crest at 1.15 s two-way travel time (TWT) is separated from the adjacent slope by a depression. Inset shows the enlarged part with the key reflectors and seismic units. Highlighted in the line are the locations of enlarged sections.

Seismic Unit 1 (SU 1):

SU 1 is the topmost unit in the upper slope, bounded by the seabed at the top and reflector S1 at the bottom (Inset, **Fig. 5**). It consists of a low-to-moderate amplitude stratified facies (SF1) (Inset, **Fig. 5**) that is continuous throughout the region (**Fig. 3a**). The thickness of this unit varies from 0.5 to 2 m (**Fig. 4a**). In water depths of 300-480 m, the unit is thicker (≥1 m; **Fig. 4a** and Inset, **Fig. 6a**), while in water depths greater than 480 m, the thickness is <1 m.

Interpretation**:** The low-to-moderate amplitude reflections likely represent hemipelagic sediments and plumites deposited from meltwater plumes. The thicker areas indicate sediment accumulation in pre-existing topographic lows (**Fig. 4a** and Inset, **Fig. 6a**).

Seismic Unit 2 (SU 2):

Unit SU 2 is bounded by reflectors S1 at the top and S2 at the bottom (Inset, **Fig. 5**). In water depths of 450–900 m, SU 2 consists of well-stratified reflections of moderate to high amplitude (SF2) (Inset, **Fig. 3b and Fig. 5**). The thickness of SU 2 varies from 1 to 6 m (**Fig. 4b**). Isolated pockets of chaotic facies (CF1) are observed within SU 2 at a water depth of ~475 m (**Fig. 3b** and **Suppl. Fig. 4**). SU 2 is not preserved above water depths of 450 m (**Fig. 4b**).

Interpretation**:** The presence of well-stratified, moderate-to-high amplitude reflections indicates the deposition of well-sorted sediments (coarse to fine) caused by turbidity currents, particularly at water depths ranging of 450-800 m. At a water depth of 475 m, an isolated pod of chaotic facies is interpreted as glacial debris. A sediment wave crest separated by a channel (**Fig. 5**) indicates the influence of along-slope contour currents, which capture particles cascading downslope and redistribute them parallel to the slope (Sarkar et al., 2011; Masson et al., 2002).

Seismic Unit 3 (SU 3):

SU 3 is bounded by reflectors S2 at the top and S3 at the base in water depths greater than 450 m (**Fig. 6b**), and by reflectors S1 at the top and S3 at the base in water depths less than 450 m (Inset in **Fig. 6a** and **Fig. 7a**). Reflector S2 is truncated by an overlying chaotic lensoid unit, and becomes untraceable in water depths shallower than 450 m.

In water depths >450 m, the lower part of SU 3 consists of continuous, parallel, moderate-to-high amplitude reflections (SF 2) that display an upward-aggrading pattern (**Figs. 6b** and **3c**). The unit thickness is nearly uniform at around 4–5.5 m (**Fig. 4c**).

In water depths <450 meters, chaotic facies (CF 1) and chaotic lenticular lobes (CF 2) are observed (**Figs. 3c** and **7a**). These lenticular lobes extend 150–600 m in the N-S direction and 500–700 m in the E-W direction, with a maximum thickness of ~10 m (e.g., **Fig. 7a**). The detachment of adjacent lenticular lobes has led to the creation of small depressions on the paleo-seabed, subsequently filled by SU1 (inset in **Fig. 6a**). The continuity of reflector S3 is affected by indentations, 1 to 5 m deep, filled with chaotic, structureless, and incoherent reflections (CF 1) (**Fig. 7a**). In the uppermost slope (water depths 390 m), the bottomset of prograding clinoforms (CF 4) (**Suppl. Fig. 5**) exhibits undulating wavy reflections. The average height of the wave is ~9 m. We have used the TOPAS profiles to map SU 3 in the Kongsfjorden TMF region, where the prograding glacial clinoforms and chaotic debris facies are distributed in a fan shape on the upper slope and are more extensive than in the interfan region (**Suppl. Figs. 6, 7,** and **Suppl. Table 4**).

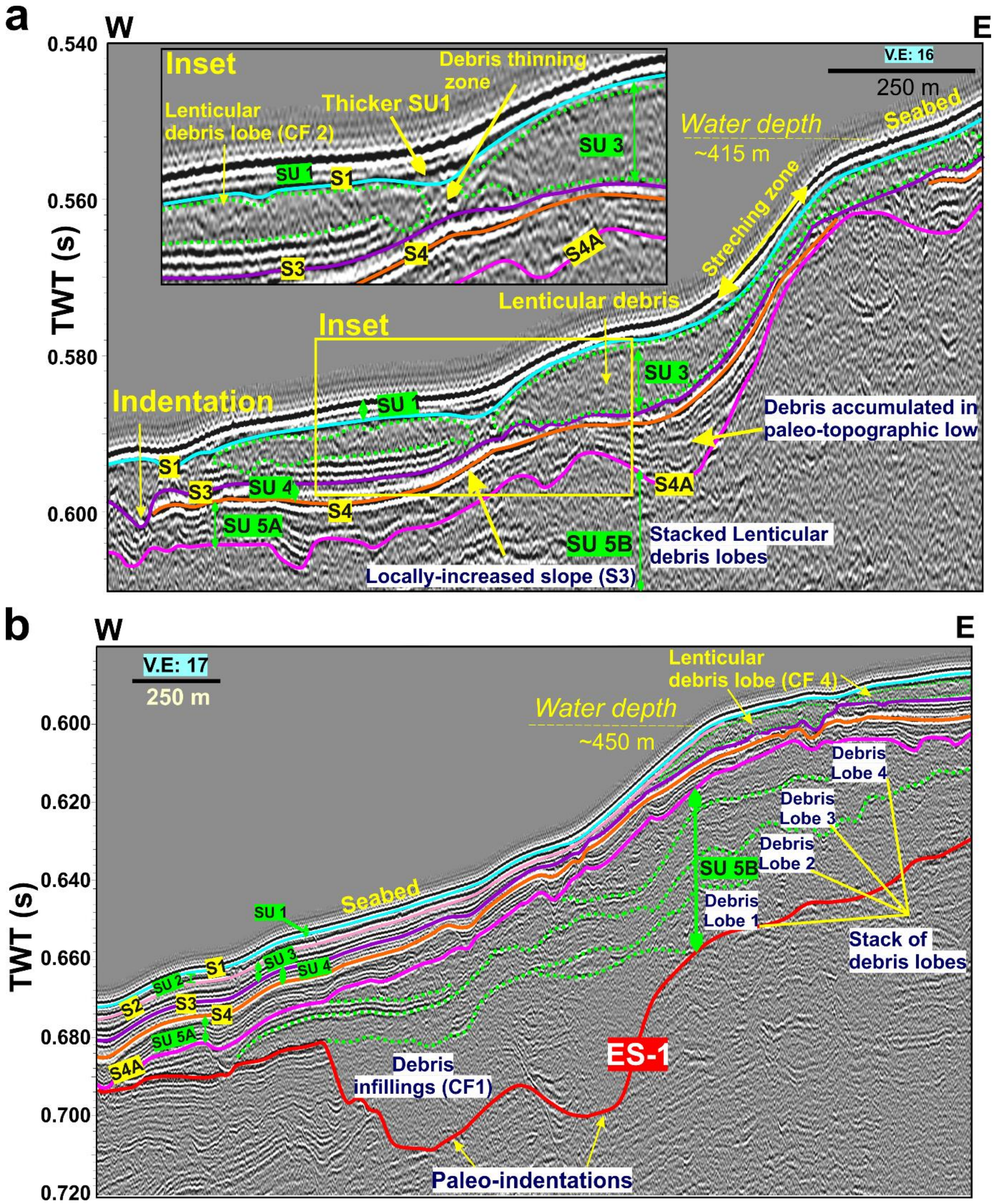

Figure 6. Slope-perpendicular SYSIF seismic profile 2.4 (location in Fig. 1c) showing various seismic facies. (a) Debris lobes of unit SU 3 thin above a locally-increased slope gradient (inset). The resulting depression is then filled by SU 1; (b) A prominent erosional surface ES-1 is filled with early debris flows and a vertical stack of lenticular debris lobes in seismic unit SU 5B. Stacked debris lobes create obstacles for younger debris lobes to overcome.

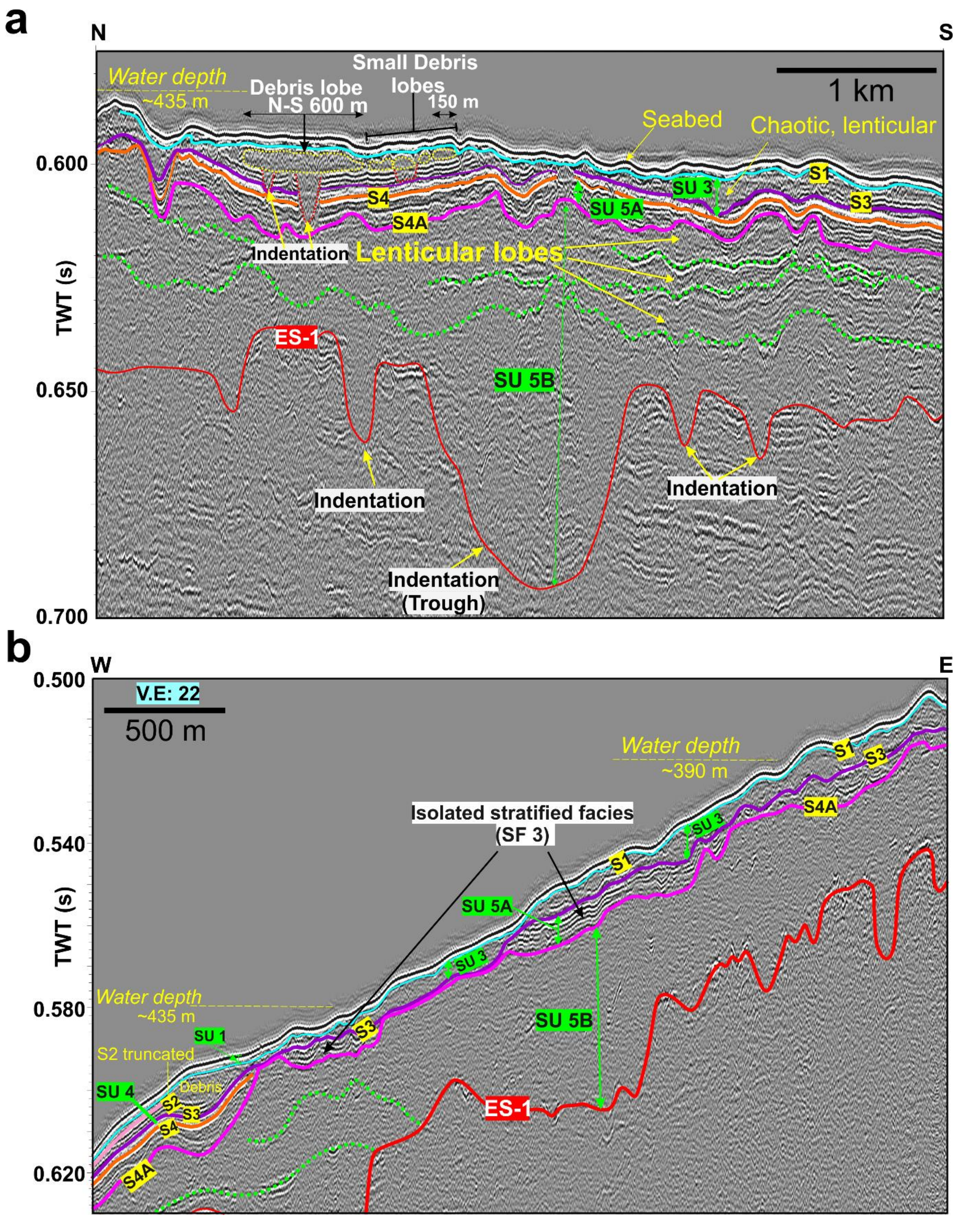

Figure 7. SYSIF seismic profiles displaying diverse seismic units and facies (line locations are shown in Fig. 1c). (a) Slope parallel SYSIF seismic profile 3.14 showing prominent indentations at the base of units SU 3 and SU 5B. They are filled by incoherent, chaotic reflection (CF1). Multiple stacks of lenticular debris lobes are present in unit SU 5B, while a single debris lobe set is seen in SU 3, (b) SYSIF seismic profile 3.1 shows isolated stratified facies (SF 2) representing remnants of turbidites (SU 5A) that were later eroded by the glacial debris flow. In addition, the SU 4 deposits are not preserved in water depths <435 m.

***Interpretation*:** In water depths less than 450 m, the chaotic facies in this unit represent glacial debris deposits. The grooves are interpreted as a result of iceberg ploughing followed by infilling with chaotic debris (CF 1) facies. The grooves bear a resemblance to the seismic expression of Late Weichselian ploughmarks observed in JR211 seismic lines and TOPAS lines by Sarkar et al. (2012) and Zhao et al. (2017), respectively. It is likely that during deposition of SU3, icebergs were carried northward by the West Spitsbergen Current, as observed during the Late Weichselian (Zhao et al., 2017). Alternatively, the grooves may suggest potential debris flow channelization, which likely contributed to the erosion process. Based on the external geometry and internal reflection, the chaotic lenticular facies (CF 2) pattern is interpreted as representing debris lobes. The thinned area between adjacent lenticular lobes is the necking zone for these debris flow lobes. The bottomsets of prograding clinoforms on the uppermost slope display wavy reflections indicating the action of northward-flowing contour currents. These currents, coupled with the eastward Coriolis deflection, redistribute the sediments as they cascade down the slope. In water depths 450–750 m, continuous, parallel reflections with high-medium amplitude (SF 2) likely indicate the presence of coarser sandy and silty sediments deposited mainly by turbidity currents, while in deeper waters (>750 m), sediment wave development is seen (**Fig. 5**).

Seismic Unit 4 (SU 4):

SU 4 is bounded by reflector S3 at the top and S4 at the bottom (Inset, **Fig. 5**). This unit consists of moderate-to-high-amplitude continuous, parallel reflections (SF 2) with the rare occurrence of incoherent semi-transparent to transparent facies (CF 1) in isolated pockets (**Figs. 3d and 8a**). The thickness of this unit is nearly uniform, ~3–4 m (Fig. 4d). The unit has undergone erosion, resulting in its absence in water depths <435 meters (Fig. 3d).

***Interpretation*:** Moderate-to-high-amplitude stratified reflections (SF 2) likely represent glaciomarine deposits with finer-grained sediments (silt or silty clay), while the isolated incoherent transparent facies (CF 1) represents debris deposits.

Seismic Unit 5 (SU 5):

SU 5 is bounded by reflector S4 at the top and S5 at the bottom (Inset, Fig. 5). The unit is further subdivided into SU 5A and SU 5B by reflector S4A (Figs. 6a, 6b, 7a, 7b, and 8a). The slope reflector S5 merges into an erosional surface (ES-1) at a water depth ~635 m.

Unit SU 5A: This unit is bounded by reflector S4 at the top and S4A at the bottom. In water depths greater than 600 m, the unit is predominantly represented by SF 2 facies (Fig. 3e and Inset, Fig. 5). In water depths of 450-600 m, SU 5A shows intercalation of chaotic facies (CF 1) and well-stratified reflections with medium and high amplitude (SF 2) (Figs. 3e, 7a, 7b, and 8a).

In water depths <450 m, isolated well-stratified (SF3) facies and chaotic lensoid facies (CF 2) are present (Fig. 3e). For example, there is chaotic lenticular facies separated by stratified facies in water depths of 400–440 m (Fig. 7b). In these water depths, SU 5A is mostly absent, with only isolated remnants preserved. Where SU 5A is absent, SU 5B is overlain by chaotic units of SU 3. The maximum thickness of the well-preserved part of this unit is ~9 m in 450–700 m water depth (Fig. 4e).

***Interpretation*:** Based on the lateral variation in the seismic facies, SU 5A shows a transition from chaotic debris to stratified deposits in water depths > 450 m. Isolated stratified reflections in water depths less than 450 m (Fig. 7b) are likely remnants of turbidites/plumites, which were not completely eroded by later glacial debris flows. The thicker parallel-bedded seismic facies that is mostly preserved at water depths of 540–700 m suggests sediment deposition from turbidity currents. The development of turbidity currents is attributed to the progressive dilution of debris flow materials as they cascade downslope.

SU 5B: This unit is bounded by S4A as the top bounding reflector and ES-1 as the base reflector (Figs. 8a and 8b). The ES-1 reflector shows indentations (**Figs. 7a, 7b**, and **Suppl. Fig. 8**). The depth of these indentations in different SYSIF lines is shown in **Suppl. Fig. 9** and the maximum and minimum depths of indentations for different water depths are presented in **Suppl. Table 5**. The paleo-indentations show V, W, and trough shapes with sidewall slope angles ranging from 9–10° to 6–8° (**Suppl. Table 5**). These indentations are filled with chaotic facies (CF 1).

This unit consists primarily of chaotic deposits (**Fig. 3f**) and is characterized by chaotic structureless transparent facies (CF 1) and chaotic-lenticular facies (CF 2) with isolated medium to high-amplitude stratified reflections (SF 2) (**Figs. 6b, 7a, and Suppl. Fig. 8**), which separate the lenticular facies. The stack of lenticular facies is predominantly observed in the water depths of 420-480 m (**Fig. 3f**). The chaotic lenticular facies overlies a structureless transparent facies that fill in the grooves. The latter shows a greater run-out (up to ~500 m water depth, **Fig. 3f**) than the lenticular chaotic sub-units. The maximum along-slope length and thickness of the lenticular facies in this unit are ~1500 m and ~20 m, respectively. In water depths of 300–420 m on the uppermost slope, there are oblique landward-dipping reflections (**Suppl. Fig. 10**). They show an apparent dip ranging from 0.8–1.43° and are characterized by chaotic internal reflections and occasional transparent facies (CF 3) (**Suppl. Fig. 10**). The lateral transition from the vertical stack of chaotic lenticular facies (**Fig. 6b**) at 420–480 m water depth to the landward-dipping debris lobes at 300–420 m water depth (**Suppl. Fig. 10**), represents the shelf-ward retreating or retrogradational stacking pattern of the debris lobes. The chaotic facies in Unit 5B thins downslope in the deeper part, transitioning to stratified SF 2 facies (2–8 m thick) in water depths greater than 600 m (**Figs. 3f and 4f**).

***Interpretation*:** On the upper continental slope below 300–500 m water depth, Unit 5B is dominated by chaotic facies, which indicates the presence of glaciogenic debris deposits. The erosional surface (ES-1) exhibits distinctive irregularity, marked by V/W-shaped grooves and erosional troughs. ES-1 is overlain by incoherent and structureless debris material (CF 1 facies). The slope-parallel alignment of thicker (>23 m) debris-filled paleo-indentations (see **Fig. 4f**) is likely a result of iceberg drifting influenced by the West Spitsbergen Current, followed by ploughing and subsequent debris infilling. Similar examples of deeper ploughmarks (> 40 m) were previously reported in the Bear Island Trough (Andreassen et al., 2008) and the East Siberian Continental Margin (Niessen et al., 2013). The trough shape (see **Suppl. Fig. 9**) of the paleo-indentations could result from the erosive action of debris flows channelled along them. Multiple layers of lenticular debris lobes accumulated on top of one another. Some lenticular lobes extended beyond this zone due to their high runout potential. The presence of eastward-dipping reflections on the uppermost continental slope (CF 3 facies) is likely a consequence of frontal obstruction caused by pre-existing debris mounds in the downslope region (**Suppl. Fig. 10**).

Seismic Unit 6 (SU 6):

SU6 is bounded by S5 at the top and S6A at the bottom (Inset, **Fig. 5**). This unit is present in >615 m water depth and is truncated by ES-1 (**Figs. 8a and 8b**) in shallower water depths. It consists of stratified SF2 facies.

***Interpretation*:** The facies in this unit is interpreted as being predominantly of glaciomarine origin.

Seismic Unit 7 (SU 7):

In water depths >650 m, SU 7 is bounded by S7 (base) and S6A (top), and represented by moderate amplitude stratified reflections (SF2) (Inset, **Fig. 5**). Slope reflector S7 merges with the erosional surface ES-2, while S6A is truncated by reflector ES-1 on the upper slope (**Fig. 8b**). Hence in <615 m water depth, SU 7 is bound by ES-2 (base) and S6A (top) or ES-1 (top), and represented by CF1 facies (**Figs. 8a and 8b** and **Suppl. Fig. 8**). Reflector ES-2 shows indentations, e.g., V-shaped groove (**Suppl. Fig. 8**).

***Interpretation*: The seismic unit SU 7 is predominantly made of glacial debris in water depths <615 m, while in deeper water, the debris grades into coarse-grained stratified SF 2 facies, most likely related to turbidite deposits/depositional processes.

Seismic Unit 8 (SU 8):

The unit is bounded by ES-2 (top) and S7A (base) in 480–615 m water depths, while in deeper water, it is bounded by S7 (top) and S7A (base) as the erosional surface ES-2 merges with the slope reflector S7 (**Fig. 8b**). The unit consists of stratified facies of high to moderate amplitude reflections (SF 2). The unit is eroded by ES-2 and cannot be tracked at <480 m water depth (**Fig. 8a** and **Suppl. Fig. 8**).

***Interpretation*:** The stratified reflections are mostly eroded in water depths less than 450 m, and in deeper waters (>750 meters), they form a wave crest, indicating the role of contour currents. These deposits can be classified as contourites.

Seismic Unit 9 (SU 9):

SU 9 is bound by ES3 (base) and S7A (top) and represented by chaotic facies CF1 (**Figs. 8a and 8b**). In deeper water (>600 m), ES3 merges with the slope reflector S7B. ES-3 shows V-shaped indentations (**Fig. 8b**).

***Interpretation*:** The V-shaped indentations observed on ES-3 are likely caused by either iceberg ploughing or debris erosion. The unit is represented by glacial debris.

4.2.3. Stratigraphic framework:

The key reflectors (S1–S7) from the SYSIF data were correlated with those identified from TOPAS data (Wiberg et al., 2022) in deeper water (~925 m water depth), where they intersected (**Fig. 1c**). The processed wavelet lengths of the SYSIF and TOPAS data are 2 and 0.2 ms, respectively. The gap between the key reflectors in the TOPAS data was greater than the wavelet of SYSIF data (2 ms). Therefore, the maximum uncertainty of picking and correlating the reflection events is ±1 ms. The age of the reflectors from the TOPAS data was derived from piston core GS10-164-09PC retrieved from the Kongsfjorden TMF region (Wiberg et al., 2022). Reflectors are assigned the following ages: S1 at ~15 ka, S2 at ~24 ka, S3 at ~38 ka, S4 at ~54 ka, S6 at ~75 ka, and S7 at ~90 ka (**Fig. 9a**). Additionally, ages for reflectors S5, S6A, S7A, and S7B were estimated at ~61 ka, ~80 ka, ~110 ka, and ~120 ka, respectively, considering the sedimentation rates provided by Wiberg et al. (2022).

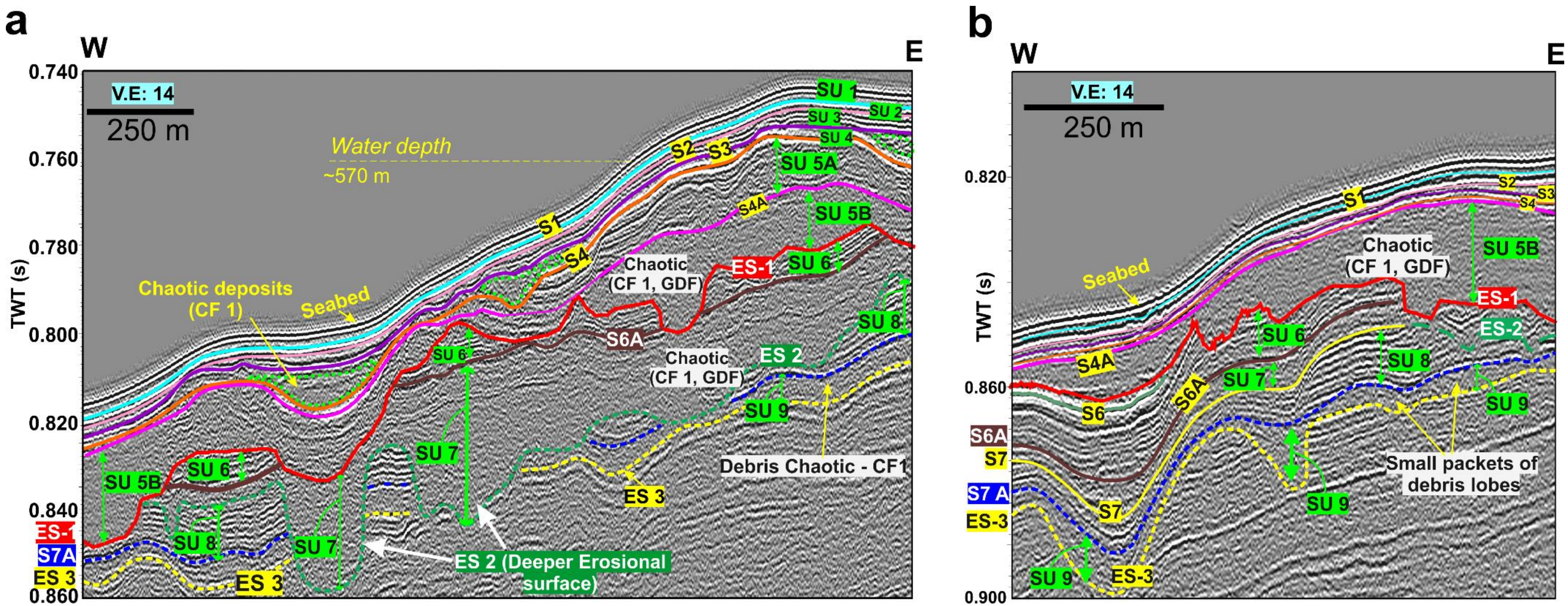

Figure 8. SYSIF seismic profiles illustrate a range of seismic facies (line locations are shown in Fig. 1c and Fig. 5). (a) Slope perpendicular SYSIF seismic profile 2.1 showing three prominent erosional surfaces (ES 1-3). The isolated chaotic facies (CF 1) is seen in unit SU 4. The erosional surfaces are overlain by chaotic debris, (b) Slope perpendicular SYSIF seismic profile 2.1 showing the termination of reflectors S6 and S7 by the erosional surfaces ES-1 and ES-2. ES-3 is the deepest erosional surface, showing the presence of grooves.

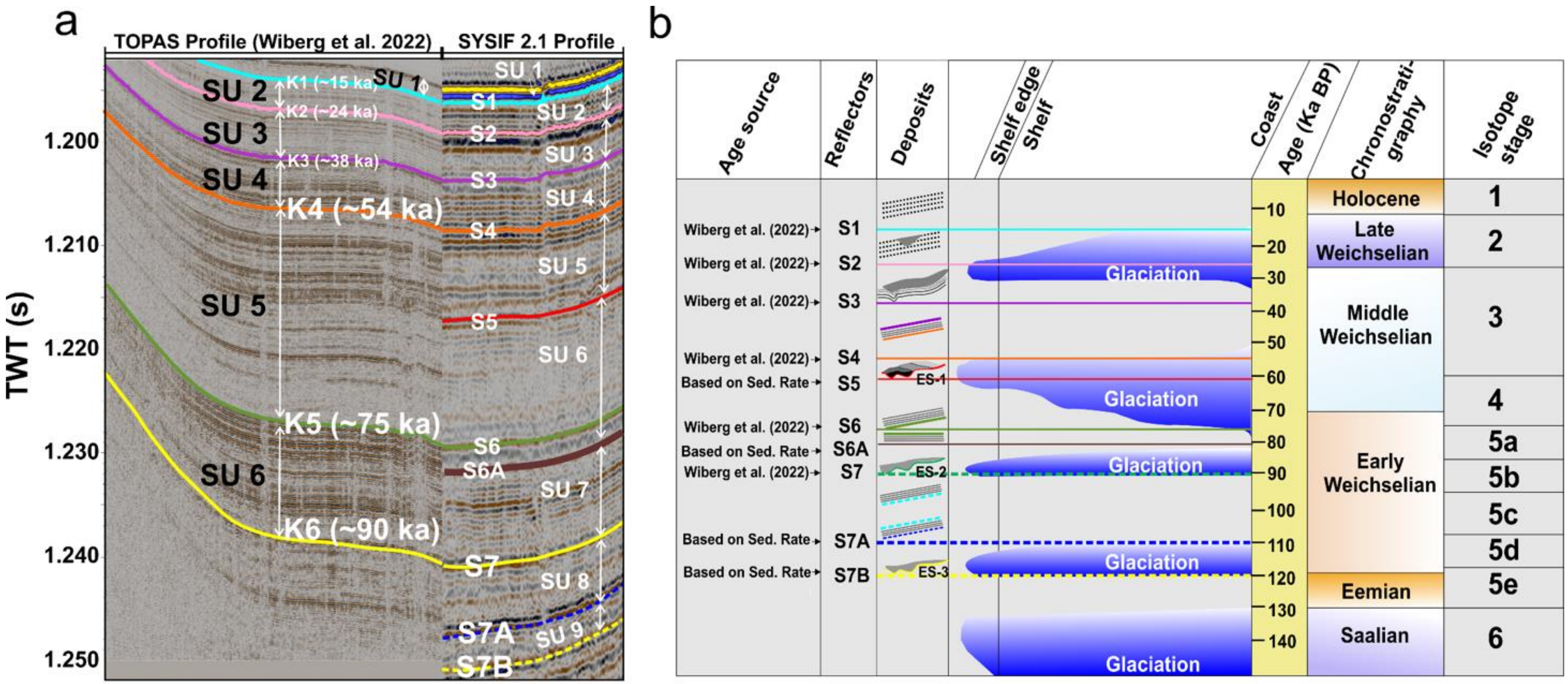

Figure 9. (a) A combined TOPAS and SYSIF seismic profile in the interfan region highlights the stratigraphic correlation (location in Fig. 1c). The ages were derived from the piston core GS10-164-09PC (location shown in Fig. 1c) retrieved at 945 m water depth in the KTMF region by Wiberg et al. (2022), (b) Correlation of SYSIF seismic horizons with different Weichselian shelf-edge glaciations. Information for coastal glaciation is obtained from Mangerud et al. (1998), Eccleshall et al. (2016), and Wiberg et al. (2022). Information on the Saalian glaciation is from Eccleshall et al. (2016) and sedimentation rate is from Wiberg et al. (2022).

4.3. Debris flow modeling with RAMMS:

The RAMMS model was calibrated to find the best-fitting rheological parameters that would produce the observed runout distance, thickness, and morphology of the modeled debris flow. It was assumed that the flow would stop at a momentum threshold of 6%, which is determined by comparing the momentum values of every grid cell to the maximum momentum sum. This threshold aligns with the recommended threshold of less than 10% in RAMMS. In this study, a 50-meter-thick and 500-meter-wide debris block was released from a till wedge at the shelf break. We varied the initial thickness and width, but the specified initial debris dimensions could generate a large lenticular debris lobe, averaging 4-5 km in length and ~5 m in height on the upper continental slope. Such a lobe would form approximately 6 to 7 km from the shelf break after flow cessation, as seen in the seismic line. Since most debris lobes are observed in the relatively steeper upper slope regions, debris flow modeling attempted to mimic the behaviour of high-strength debris flow considering yield strengths ranging from 100 to 2000 Pa (Talling, 2013). High-strength debris flows (~100 Pa to >1 kPa) generally occupy steeper gradients and remain closer to their source area, while flows with intermediate strengths (5-100 Pa) can travel down to gentler slopes (Talling, 2013).

The simulation results show various potential runout distances, thicknesses, and speeds for submarine debris flows in the interfan region. **Fig. 10a–d** show a simulation where the debris flow yield strength is assumed to be 2 kPa. The debris flow originates at the shelf break and lasts for approximately thirty minutes before coming to a halt on the upper slope. Five minutes after its release from the shelf break, the debris flow mass starts to elongate, and the debris head surges ahead in the form of a lobate geometry with an estimated maximum velocity of 5 m/s. The debris flow typically shows a bulbous head and a tapering tail. There is a gradual reduction of mass in the flow's tail and the progressive accumulation of debris material in the head region. The flow front finally stops at the lower gradient part of the slope, ~6 km away from the point of origin. The cessation of the debris flow onto the seafloor is influenced by multiple factors, including a decrease in slope angle from 4° to less than 0.5° and the cohesive properties of the flow, calibrated to correspond to a yield strength of 2 kPa.

In the case of the flow with a yield strength of 100 Pa, the flow ceases at a distance of 8.5 km from its origin, reaching the gentler part of the slope (**Fig. 10e–h**). Debris flows with lower yield strength tend to break up more easily than those with higher yield strength. The final state shows several localized features with an undulating morphology compared to the final morphology of the debris flow in the case of yield strength assumption of 2 kPa. The undulating topography of the debris lobe is due to local slope variations of the substrate. The debris mass mostly accumulates on gentler sections while thinning out on steeper sections as the flow velocity is relatively higher in those regions. Cohesive lenses and stretched/thinned debris with internal bulges are observed in the seismic data (Inset, **Fig. 6a**). The modeling aids in comprehending the potential reasons for their creation.

In a separate experiment, we investigated the potential of a barrier to halt the debris flow. When the energy needed to overcome the barrier is lacking, the flow front is halted by the barrier, forming a thicker head leaning against it and a landward-dipping tail (**Suppl. Fig. 11a–d**). Additionally, in another experiment, we demonstrated the infilling of a north-south trending ploughmark by debris. The debris flow exhibits a distinct tongue-shaped outline as it advances toward a ploughmark (**Fig. 11a-f**). The infilling of the ploughmark initiates when the debris flow encounters the groove, progressively extending laterally along the groove as the filling process proceeds.

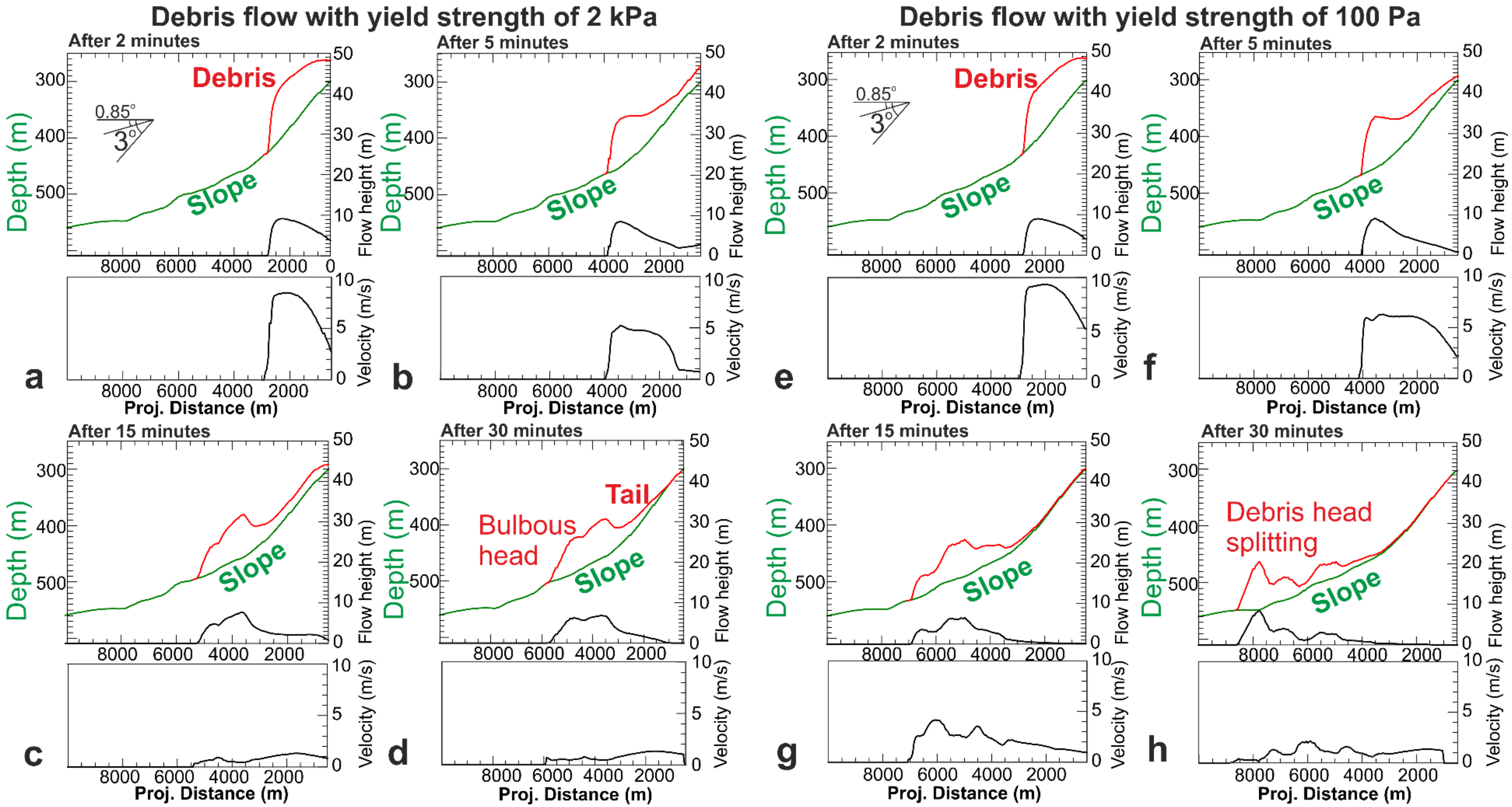

Figure 10. Evolution of debris flow after being released as a block at the shelf break, considering a yield strength of 2 kPa (a-d) and 100 Pa (e-h). The slope topography was generated by tracking the ES-1 horizon. (a) The debris flow mass 2 minutes after its release shows a high initial flow velocity of 9 m/s, b) After 5 minutes, the debris mass is shifted towards the flow head, and the tail thins out, c) After 15 minutes, a distinct bulbous head is formed, d) After half an hour, the debris lobe reached approximately 6 km away from the initial release site after flow cessation, e) Two minutes after release, the debris flow mass exhibits an initial flow velocity of 10 m/s, f) The debris mass undergoes a transformation in shape after 5 minutes, leading to a lensoid shape, g) After 15 minutes, the lensoid debris mass surges ahead at 5-7 m/s, h) Thirty minutes later, the debris flow mass begins to develop distinct internal bulges separated by thinned zones. The debris lobe comes to a halt approximately 8.5 km away from the initial release site.

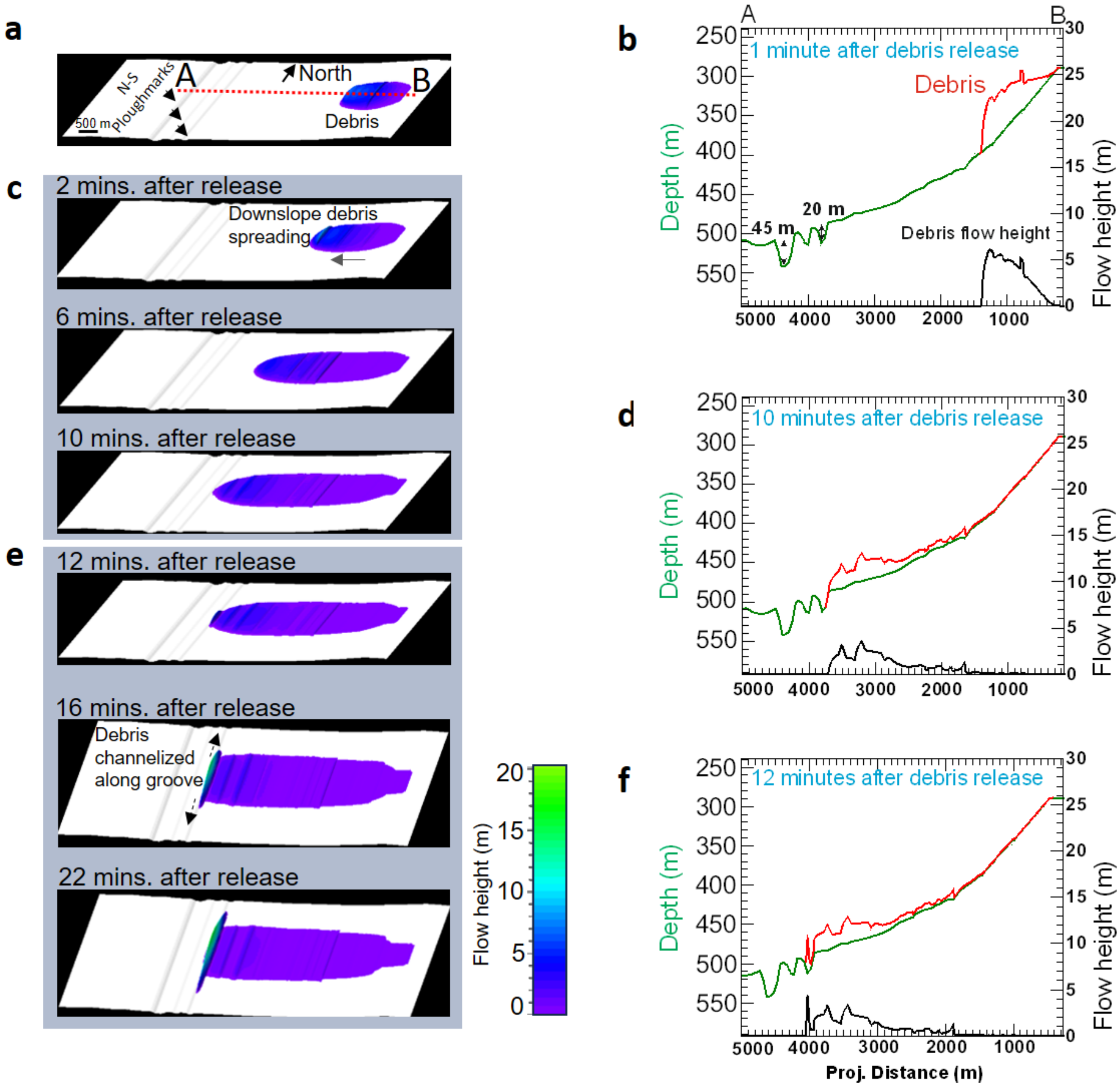

Figure 11. RAMMS simulation showing ploughmark infilling. a) Three-dimensional depiction of a westerly dipping slope showcasing the release of debris mass from the shelf break, with three N-S aligned ploughmarks approximately 4 km away from the shelf break, b) Section AB presents the profile of the slope and ploughmark grooves, c) Visualization of debris flow spreading and changes in debris flow height at 2, 6, and 10 minutes post-release, d) Profile section illustrating the debris snout reaching the brink of a ploughmark, e) Illustration of debris filling the ploughmark on the most landward side of the slope, f) Profile section displaying debris infilling the ploughmark.

5. Discussion

5.1 Glacial history and paleo-depositional environment

The following sections provide an overview of the evolution of the glacial ice sheet in the interfan area between Kongsfjorden and Isfjorden TMFs over the last 2.7 million years. They discuss changes in paleo-depositional environments and glacial dynamics based on the analysis of variations in seismic facies across various seismic units.

Period: > 2.7 Ma

The parallel continuous to semi-continuous low to medium-amplitude well-stratified facies in IU-5 in the outer shelf suggest sedimentary strata, while the incoherent facies in IU-6 represent the crystalline rocks (**Fig. 2**). In the upper slope, the northward flow of the West Spitsbergen Current (WSC) led to upslope climbing contourite deposition with a distinct wavy pattern, occurring in a low-energy environment conducive to pelagic and hemipelagic sedimentation (**Fig. 2**).

Period: 2.7-1.2 Ma

The sedimentary strata deposited between 2.7 million years (R7) to 1.2 million years (R4A) shows climbing-up wavy sedimentary succession in the upper slope that thins out towards the shelf break and outer shelf (**Fig. 2**). The initiation of Northern Hemispheric glaciations around 2.7 Ma, exemplified by the shelf edge glaciation in northwestern Svalbard, led to the formation of the Sjubrebanken Fan at ~2.5-1.2 Ma (Sarkar et al., 2011). However, during this period, there were no indications of fan development in the Kongsfjorden area.

Period: < 1.2 Ma

The chaotic wedges above the R4A reflector (1.2 Ma) indicate the presence of glaciogenic deposits formed by the advancing ice during the basinward progression of the ice sheet in the interfan area. Shelf progradation is evidenced by the prevalence of lensoid packages alternating with moderate to high-amplitude basinward advancing clinoforms downlapping reflector R4A (**Fig. 2**). These lensoid packages denote glaciogenic debris, while the moderate-amplitude reflections result from the draping of hemipelagic sediments and plumites, deposited through suspension fallout from meltwater plumes, and sand-rich turbidites settled from turbidity currents. The URU on the shelf marks a substantial erosion of underlying strata and shelf progradation above the URU. **Suppl. Fig. 12a-c** schematically depicts the initial ice sheet advancement, resulting in the erosion of underlying sedimentary units, creating the URU and transporting glacial debris to the outer shelf and shelf break. Shelf edge glaciations at 1.2 Ma and in subsequent cycles resulted in the formation of prograding glacial wedges. The presence of prograding sequences on the outer shelf implies the availability of accommodation space, while the inner shelf region was susceptible to either erosion or sediment bypass. In the Kongsfjorden TMF region, R4A (~1.2 Ma) serves as the base of lensoid debris flow packages extending to the upper slope, indicating the initiation of ice-streaming along the Kongsfjorden Trough (**Suppl. Fig. 2b**). However, the interfan region shows moderate progradation compared to the fan development in the KTMF. Between 1.20 Ma (R4A) and 0.074 Ma (X1), the shelf witnessed multiple glacial advancements, evident in distinct sets of oblique westward-dipping lensoid debris packages. Due to the lack of age constraints in the shelf and the difficulty in tracking regional reflectors on the upper slope and outer shelf, dating multiple episodes of glacial advancements and retreats remains challenging. However, by utilizing the available age reflectors, we correlate the prograding clinoforms downlapping onto reflectors R4A (1.2 Ma) and R2 (0.42 Ma) to the glaciations of Mid-Pleistocene and Early Saalian, respectively.

Suppl. Fig. 13a illustrates a hypothetical scenario where the ice sheet retreats from the shelf break area. During this period, there might possibly be shorter pauses in ice retreat, resulting in the deposition of retreat moraines during glacial stillstands on the outer shelf. On the distal slope, plumites became more prevalent due to the diminished supply of glacial debris and abundant meltwater causing dilution (Vorren et al., 1990). These plumites may locally become unstable if they accumulate rapidly over steeper slopes and are transported downslope by turbidity currents. **Suppl. Fig. 13b** depicts the readvancement of the ice sheet towards the shelf break. As the ice advances, it erodes the existing deglacial sediments. The top of the prograding glaciogenic sequence in units IU-4 –2 is truncated by reflector M (**Fig. 2**), indicating such glacial erosion during re-advance of the ice sheet.

On the shelf break and upper slope, the shallowest seismic unit IU-1 exhibits prograding clinoforms, suggesting ice sheet advancement to the shelf break. Reflector W marks the base of this unit, truncating X1 (~75 ka) on the upper slope, indicating Unit IU-1 is <75 ka. The distinct episodes of glacial advancements and retreats in this unit cannot be resolved with the air gun seismic data since it lacks the resolution required to decipher the intricate stratigraphic patterns in the upper slope. To address this limitation, SYSIF seismic lines from the upper continental slope were interpreted to reconstruct the glacial (Weichselian) history during the last 120,000 years and glaciomarine sedimentation patterns.

5.2 Weichselian glacial history and depositional environment

On the slope, we have documented an alternation of chaotic debris and stratified deposits separated by prominent erosional surfaces ES 1–3. These features help in reconstructing glacial advances and retreats from the shelf break. The grounded ice sheet at the shelf break marks the maximum basinward advance during a specific glaciation. During an ice advance, the floating part of the ice sheet is prone to calving events. Calving events are likely to occur when the ice sheet becomes unstable during a highly dynamic growth stage. Substantial calving events are likely during the peak of glaciations, with deep-keeled icebergs likely to form in regions where paleo-ice streams were once active. The deep-keeled icebergs gouge the uppermost slope, leaving behind ploughmarks. A submerged till wedge is formed at the shelf edge by the grounded ice sheet during periods of shelf-edge glaciation. The glacial debris cascades downslope from the unstable sediment wedge established in front of the shelf-based ice sheet. However, when the ice sheet retreats from the shelf break, the supply of glacial debris diminishes, and small volumes of debris are deposited/dumped on the upper slope. With the continued retreat of the ice sheet towards the inner shelf, a significant release of meltwater plumites occurs, transported by currents along the upper slope and/or downslope as turbidity currents. Turbidites from these meltwater deposits are deposited over the underlying debris units. Based on this interpretation, the glacial history of the margin was verified (**Fig. 9b**).

5.2.1 Early Weichselian 120–75 ka (SU-9, SU-8, SU-7, and SU-6)

The base of unit SU-9, ES-3 shows V-shaped indentations and is covered by debris materials (SU-9) and stratified deposits (SU-8) in vertical succession. The indented surface is likely a product of ploughing by deep-keeled icebergs. These icebergs are presumed to have originated from ice streams situated farther south and were subsequently carried by the northward-flowing West Spitsbergen Current. Debris materials, which descended downslope from a grounded ice sheet at the shelf break of the interfan region, filled in these grooves.

Alternatively, the grooves may have resulted from erosion associated with debris flow. Owing to constraints in tracking ES-3 across the study area, we are unable to make judgments regarding the lateral continuity or extent of the indentations. Specifically, we cannot determine whether they are slope-perpendicular gullies or nearly slope-parallel iceberg ploughmarks. ES-3 laterally correlates with the reflector S7B (~120 ka). Unit SU-9, which is bounded by ES-3 and S7A (~110 ka) and represented by debris, corresponds to a period of shelf-edge glaciation during ~120–110 ka. SU-8 (~100-90 ka) shows stratified deposits, such as plumites and turbidites, deposited by meltwater-driven turbidity currents that likely formed during the glacial retreat from the shelf break to the inner shelf when meltwater supply was abundant. This interpretation is in accord with the ice sheet reconstructions by Mangerud et al. (1998) and Ingolfsson & Landvik (2013) that suggest that the shelf edge glaciation outside Isfjorden ceased around 108 ka.

The base of seismic unit SU-7 shows a prominent erosion (ES-2) and correlates with the slope reflector S7 (~90 ka). ES-2 shows V-shaped indentations, likely representing ploughmarks created by icebergs or erosion caused by debris flow. The presence of chaotic debris flow in SU-7 on the uppermost slope provides evidence of debris supply by a grounded ice sheet at ~90 ka. The reflector S6 within the overlying turbidite unit SU-6 is dated to 75 ka, while the top bounding reflector of SU-7 (S6A reflector) is dated to approximately 80 ka based on the average sedimentation rate. The stratified deposits of unit SU-6 suggest a subsequent shift in the depositional environment. Alexanderson et al. (2018) identified interstadial deposits at the Kongfjordhallet in the outer Kongsfjorden, dating them to 85 ka during a period of relatively ice-free shelf conditions. Based on this data and the nature of seismic facies, the well-stratified reflections of Unit SU 6 (bounded between S6A and S5) likely represent plumites and turbidite sediments of deglacial origin (85–75 ka).

5.2.2 Early Mid-Weichselian 75–54 ka (SU 5B and SU 5A)

The base of unit SU 5B is marked by an erosional surface ES-1. This surface cuts the underlying strata, including reflector S6 (~75 ka), but merges with reflector S5 (~61 ka). Additionally, ES-1 shows iceberg ploughmarks. In the slope of the interfan area, the ploughmarks are deep (maximum depth ~55 m) and mainly occur in the water depth interval of 410–520 m, while a few are found around 600–700 m depths. The infilling glaciogenic debris deposits of Unit SU 5B suggest the sediments were released from a grounded ice sheet on the upper slope.

The overlying unit SU 5A, bound by S4A at its base and S4 (~54 ka) at its top, shows a transition from chaotic facies to stratified beds with intermittent interbedding of debris in water depths 450–600 m. This transition implies the dilution of glaciogenic debris as meltwater content increases. Units SU 5B and 5A represent deposition under the shelf edge glaciation spanning 61–54 ka, equivalent to MIS 4. Wiberg et al. (2022) proposed shelf-edge glaciation between 70–54 ka, since glacial debris flows are observed after ~75 ka; however, based on SYSIF data analysis, a peak in iceberg calving occurred around 57–61 ka, suggesting that ice grounding likely preceded the peak period of ice sheet calving and an enhancement in ice flux during ~57–61 ka. This period is considered as the most extensive Weichselian glaciation in the Barents and the Kara Seas prior to the LGM, denoted to represent MIS 4 (Svendsen et al., 2004).

5.2.3 Mid-Weichselian (54–38 ka) unit SU-4:

Unit SU 4, bounded by reflectors S3 (~38 ka) and S4 (~54 ka), shows moderate-to-high-amplitude stratified reflections (SF 2) in water depths <450 m. The glacial debris lobes are conspicuously absent at these depths, except for a few isolated debris pockets. The moderate-amplitude stratified facies of this unit represents deposition from meltwater plumes generated by an ice sheet situated further landward from the shelf break. This ice sheet location resulted in a significantly reduced glacial debris supply and occasional turbidity currents when the deposition of plumites/glaciomarine sediments on the steeper upper slope became unstable and was transported downslope as they mixed with ambient water. Although the SYSIF lines could not resolve this unit at water depths <420 m, the sediments retrieved from shallow core at the uppermost slope suggest a transition from sand and pebbly clay to overlying silty clay (Bohrmann et al., 2017, **Suppl. Fig. 14 and 15 and Suppl. Text 1.**) This transition indicates a shift in the depositional environment, from debris flow to turbidity currents at the uppermost slope as the ice sheet started to retreat from the shelf break and debris supply diminished.

5.2.4 Middle to Late Weichselian (38–24 ka)

Unit SU 3 in the shallower depths (<450 m water depth) consists of chaotic facies (CF1) and lenticular facies (CF2) interpreted as glacial debris lobes, indicating the reestablishment of a grounded ice sheet at the shelf break supplying glacial debris on the upper continental slope. This observation is supported by the results from gravity cores from cruise MSM57 (Bohrmann et al., 2017, **Suppl. Fig. 14 and 15**), which show the predominance of pebbly clay related to poorly sorted debris flow materials. Based on seismic facies and information from gravity cores, the SU 3 unit represents glacial sediments deposited at the maximum extent of the grounded ice sheet during the LGM. The Kongsfjorden TMF region exhibits fan-shaped debris distribution fed by a paleo-ice stream and extensive debris runout, as shown in **Suppl. Fig. 6** and **Suppl. Fig. 7a-c**. In the interfan region, the asymmetric waves on the uppermost slope at the toe of prograding clinoforms could indicate upslope migrating sediment waves (**Suppl. Fig. 5**) that migrate to the east of the northward flowing West Spitsbergen Current, indicating intermittent influence by this current.

5.2.5 Late Weichselian (24–15 ka)

The moderate-to-high-amplitude SF2 facies in SU2 (24–15 ka) indicates coarse-grained sandy/silty sediments deposited in water depths >450 m. During the ice retreat period, a substantial amount of plumites were produced and transported by currents on the slope over long distances. As the ice sheet started to retreat from the shelf break, the uppermost slope saw a diminishing influence of debris. Over time, the deposited plumites became unstable and were subsequently transported downslope as debrites and/or turbidites, likely driven by substantial influxes of water.

5.2.6 Late Weichselian and Holocene (<15 ka)

The youngest unit SU1, which consists of low-amplitude stratified SF1 facies, indicates the predominance of hemipelagic sediments. The topmost retrieved sediments in the gravity cores (**Fig. 1c**) on the uppermost slope consisted mainly of silty clay to clay, overlying pebbly clay (Bohrmann et al., 2017, and also see **Suppl. Figs. 14 and 15 and Suppl. Text 1**). In some cores, the clay layer is absent, possibly due to the winnowing effect of the West Spitsbergen Current.

Following the retreat of the ice sheet into the fjords, there was a period during which the current on the upper slope was likely much slower. This period probably lasted until the initiation of the Bølling–Allerød interstadial, when the West Spitsbergen Current became stronger. Slubowska-Woldengen et al. (2007) suggested that an inflow of warm Atlantic Water began during the Bølling–Allerød interstadial from ~14-13 ka. Therefore, the current began reworking the seafloor sediments more vigorously, coinciding with the increased inflow of warm Atlantic Water.

5.3 Glaciogenic debris flow

Seismic units SU 5A, SU 5B, and SU 3 are dominated by debris flow deposits on the uppermost slope. These debris flows originated at the shelf break near the till wedge in water depths of 290–300 m and cascaded down the slope to depths of 450–500 m. The ability of debris flows to travel long distances depends on the presence of a thin, lubricating water layer at the base of the flow (Sobiesiak et al., 2018). This water layer reduces friction between the debris flow and the seafloor, preventing the transfer of shear stress from the flow to the substrate. For instance, in the Kongsfjorden TMF region, the meltwater supply and sediment flux were likely higher than in the interfan region.

Consequently, there was a greater debris runout distance compared to the interfan area (**Suppl. Fig. 7a**). As the front of the debris flow moves through the surrounding water, a combination of front pressure and lift forces allows a layer of water to intrude beneath the front of the flow. This process is known as hydroplaning (Mohrig et al., 1999). Hydroplaning can cause the front of the flow to accelerate, leaving behind a stretching zone. This stretching can detach the hydroplaning head, forming an outrunner lobe (Ilstad et al., 2004).

Unit SU 5B contains chaotic debris flows that lie above an irregular and heavily grooved erosional surface (ES-1). V-shaped indentations (15–55 m deep) at the base of unit SU 5B below water depths of 400–550 m suggest that icebergs ploughed the seafloor (Stage-I in **Fig. 12**). For example, a NNW-SSE trending indentation filled with debris suggests that initial iceberg ploughing was followed by subsequent debris infilling. When debris flows descend, these indentations trap the debris (Stages-I and II in **Fig. 12**). The debris cannot advance beyond the indentations until the deep indentations are filled in. The trough shape of ES-1 is indicative of erosion (**Suppl. Fig. 9**). Debris flow modeling indicates that the ploughmarks can trap debris cascading downslope, causing the flow to be channelled along the slope-parallel groove (**Fig. 11**). The debris flow can also erode the substrate. The depth of substrate erosion depends on factors such as the strength of the flow and the shear stress at the base. Erosion occurs when the shear stress exceeds a certain threshold value. The loss of basal lubricating water layer can lead to enhanced coupling between the debris flow and the substrate, leading to free-slip condition. Without a lubricating basal water layer, the shear stress at the base of the debris flow is transferred directly to the seafloor, causing erosion and incorporating substrate material into the flow. Hiscott and Aksu (1994) showed that the snout of a large debris lobe can be very erosive. The interaction of debris flow with the substrate, and the transfer of mass from the substrate to the debris flow caused by entrainment is critical for the change in momentum of the flow. Incorporating substantial amounts of substrate material, such as clay, may increase cohesive behavior, enhance viscosity, and reduce debris flow mobility. For example, Talling (2013) showed that 1-m thick debris flow over a 0.1-degree gradient slope will increase in bulk flow velocity as the mud content increases from 1 to 6%; however, flow velocity decreased with 10% clay volume as viscosity becomes a dominant factor.

In Stage-III as illustrated in **Fig. 12**, numerous debris flow lobes developed and accumulated in a vertically aggrading manner while the ice sheet was grounded at the shelf break. The stacked debris lenses act as obstacles, influencing antecedent flow behaviour. Subsequent low-volume cohesive debris flows (due to dwindling debris supply) get trapped behind the frontal obstruction. This results in a unique retrograde stacking pattern as the younger debris stacks upslope and progresses from deeper to shallower depths.

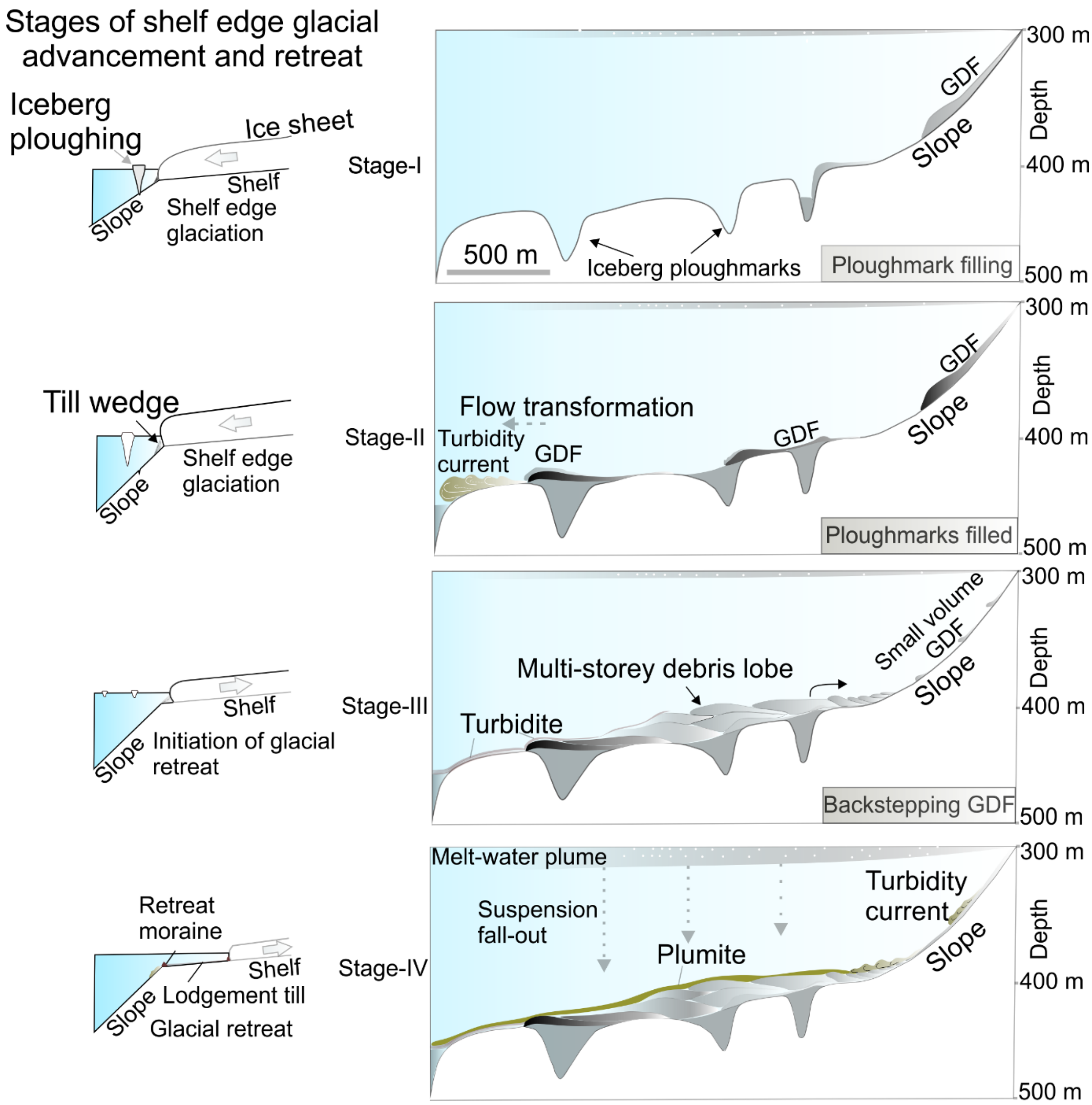

Figure 12. Schematic cartoon illustrating the patterns of glacial debris filling an erosional surface on the upper slope in relation to the position of the ice sheet at the shelf break. Stage-I depicts ploughmarks formed by deep-keeled icebergs during a major calving episode. At Stage-II, early glacial debris flows (GDFs) originated from the shelf edge, cascading downslope and filling the grooves. During Stage-III, multiple debris flow lobes emerged and stacked up in a vertically aggrading manner when the ice sheet remained grounded at the shelf break. This filling pattern could be applied to explain the debris-stacking pattern observed in unit 5B, as shown in Figs. 6b and 7a. As the debris supply diminishes, a retrograde backstepping of small-volume debris is observed. The retreat of the ice sheet from the shelf break during Stage-IV resulted in a decrease in debris supply, leading to the deposition of a smaller volume of glacial debris lobes on the upper slope. Enhanced meltwater supply generates plumites.

Debris flows can become diluted and transform into high- and low-density turbidity currents (e.g., Stage-II in **Fig. 12**). The stratified layers of unit 5A in water depths 500–700 m are juxtaposed against the chaotic facies in 300–450 m water depths. The stratified facies in unit 5A, in the distal part of the debris, marks the transition to turbidite sediments. The transition from debris flows to turbidites in a sedimentary environment can occur due to a decrease in the ratio of sediments and water. The internal processes within debris flow can also lead to flow transformation. For example, the hydroplaning debris flow snout is sometimes thinned and stretched. The stretching zone is also prone to interaction with the basal lubricating water layer, leading to cracks at the base of the flow due to increased pore pressure (Ilstad et al., 2004). These cracks allow water to penetrate the debris flow, diluting its base and the head of debris flow, reducing its shear strength, and forming a turbidity current (Hampton, 1972). These currents exhibit Newtonian fluid behaviour and have zero yield strength. The higher energy and greater fluid mobility associated with turbidity currents enable the transport of finer-grained sediments over longer distances.

6. Summary and Conclusions

The interpretation of air gun seismic data has yielded valuable stratigraphic insights for the first time, revealing the extent of the upper regional unconformity (URU) from the outer shelf to the shelf break region in the interfan. The post-URU geological succession indicates accretion of glacial materials extending the shelf break to its present-day position (post 1.2 Ma). Sarkar et al. (2011) suggested that a topography-constrained ice stream switched from northwest Svalbard to the Kongsfjorden between 1.5 and 0.99 Ma. The age constraints from the MeBo 126 drill hole and reinterpretation of existing seismic lines indicate that the ice stream switching event occurred approximately 1.2 Ma, coinciding with the Mid-Pleistocene Transition. At that time, the increase in ice sheet thickness exceeded the topographic barrier created by Prins Karls Forland, enabling the westward flow of ice along the shortest and steepest path, thus forming the Kongsfjorden cross-shelf trough. In the interfan region between Kongsfjorden and Isfjorden cross-shelf troughs, the ice sheet expanded to the shelf break approximately 1.2 Ma, resulting in the erosion of pre-existing strata and the progradation of the margin, delivering glaciogenic debris at the shelf break. Following this, multiple cycles of deglaciation and shelf edge glaciations occurred, leading to erosion and the development of basinward advancing clinoforms. Examples include shelf edge glacial advances during the Early Saalian period (~0.42 Ma ago) and the Weichselian period. The exact number of these cycles could not be determined in this study due to the lack of age controls in the shelf region except for the Weichselian cycles.

Based on the high-resolution (SYSIF) seismic dataset, four glacial advances to the shelf-edge off Prins Karls Forland were identified during the Weichselian period. They were dated to the earliest phase: ~120–110 ka, second phase: ~90 ka, third phase: ~61–54 ka, and the fourth phase (LGM): ~24 ka. The third phase is relatively shorter compared to the known timing of 70–54 ka due to a prominent erosion and calving phase at ~61 ka, which removed evidence of the earliest part of glacial sedimentation. This phase also witnessed the maximum runout of glacial debris flows, reaching water depths of up to ~600 m. In contrast, the LGM shelf edge glaciation witnessed glacial debris flows extending onto the upper slope down to ~410 m water depths.

The findings from the marine domain help to resolve existing discrepancies associated with the Weichselian glacial history. Eccleshall et al. (2016) suggested that the expansion of ice sheets to the shelf break occurred during MIS 5b (93–83 ka), while previous models did not consider this expansion. The new results support this interpretation, as there is evidence of glacial debris filling at ~90 ka, indicating that the ice sheet expanded to the shelf break at this time. This interpretation also agrees with the observations of Wiberg et al. (2022), who suggested the presence of glacial debris resulting from a ~90 ka shelf-edge glaciation. Eccleshall et al. (2016) suggested that the ice sheet did not reach the shelf break during MIS 4 (75–50 ka). The results from this work, however, contradict this suggestion, and we infer a peak in ice flux during a shelf-edge glaciation during ~61–54 ka.

Lateral and vertical changes in seismic facies were used to infer spatial and temporal changes in the glaciomarine depositional environment that were linked to multiple cycles of shelf-edge glaciations in the margin. During maximum glacial expansion to the shelf break, iceberg calving caused ploughing of the seafloor. Iceberg calving likely occurred from areas of ice streaming further south, and they were transported to the interfan region by the northward-flowing current. The grounded ice sheet at the shelf break during its maximum extent supplied debris that cascaded downslope, depositing lensoid debris lobes on the upper slope in a vertically aggrading manner. SYSIF seismic images and debris flow simulations provide insights into glacial debris travel distance and evolution in the interfan. High-strength flows occupied steeper slopes with shorter runout distances, while lower-strength flows travelled further and separated into smaller lensoid lobes due to local slope variations. Modeling also highlights the oblique, landward-dipping geometry of debris flows that emerge when they encounter an obstacle they cannot bypass. The retrograde backstepping of small-volume debris flows could result from the progressive reduction in debris supply as the ice sheet began to retreat, as well as from isostatic adjustments of the slope, such as the collapse of the fore bulge and the isostatic rebound occurring during the ice sheet's retreat, leading to a less steep slope. The seismic data revealed that debris flows transitioned into stratified deposits, such as turbidites, as they evolved into turbidity currents. Potential factors for this transformation are a decrease in sediment supply, an increase in meltwater content, and internal processes within the debris flow, such as hydroplaning and stretching, introducing cracks that allow water infiltration into the debris lobes.

Author contributions

AT and SS conceptualized the study. TAM led the seismic expedition and acquired SYSIS seismic lines with assistance from SK. SK processed the SYSIF seismic data. HH collected the TOPAS line and studied the GC10-164-09PC core. AT and SS analyzed the seismic data and developed the interpretation framework. AT wrote the manuscript with contributions from all authors. SS supervised AT.

Declaration of competing interest

The authors declare that they have no known competing financial interests or personal relationships that could have appeared to influence the work reported in this paper.

Acknowledgments

AT acknowledges the support of a PhD scholarship from the Ministry of Education, India. SS acknowledges funding from the Science and Engineering Research Board (SERB Act 2008), through the Earth and Atmospheric Science Program Start-up Research Grant (SRG/2019/001072). SS also extends appreciation to DST FIST (Grant SR/FST/ES-I/2018/25) for infrastructure support and to Shearwater Geoservices (https://www.shearwatergeo.com) and Paradigm/Emerson for providing seismic processing software, to IHS Kingdom (https://kingdom.ihs.com/) and to Eliss (https://www.eliis-geo.com/paleoscan) for offering educational software licenses to the Indian Institute of Science Education and Research, Pune. Seismic data acquisition was supported by UK Natural Environment Research Council grants NE/H002732/1 and NE/H022260/1. Timothy Henstock is acknowledged for his leadership in onboard air gun seismic data acquisition. Graham Westbrook made the case for taking SYSIF to the west Svalbard margin. We thank our deceased colleague Bruno Marsset for his critical contributions to SYSIF data acquisition.

References

Alexanderson, H., Henriksen, M., Ryen, H.T., Landvik, J.Y., Peterson, G., 2018. 200 ka of glacial events in NW Svalbard: an emergence cycle facies model and regional correlations. Arktos 4(1), 1–25. https://doi.org/10.1007/s41063-018-0037-z

Alexandropoulou, N., Winsborrow, M., Andreassen, K., Plaza-Faverola, A., Dessandier, P.-A., Mattingsdal, R., Baeten, N., Knies, J., 2021. A Continuous Seismostratigraphic Framework for the Western Svalbard-Barents Sea Margin Over the Last 2.7 Ma: Implications for the Late Cenozoic Glacial History of the Svalbard-Barents Sea Ice Sheet. Frontiers in Earth Science 9 (May). https://doi.org/10.3389/feart.2021.656732

Andreassen, K., Laberg, J.S., Vorren, T.O., 2008. Seafloor geomorphology of the SW Barents Sea and its glaci-dynamic implications. Geomorphology 97, 157–177.

Bartelt, P., Valero, C.V., Feistl, T., Christen, M., Bühler, Y., Buser, O., 2015. Modelling cohesion in snow avalanche flow. Journal of Glaciology 61(229), 837–850. https://doi.org/10.3189/2015JoG14J126

Bohrmann, G., Ahrlich, F., Bergenthal, M., Bünz, S., Düßmann, R,. Ferreira, Ch., Freudenthal, T., Fröhlich, S., Hamann, K., Hong, W.-L., Hsu, Ch.-W., Johnson, J., Kaszemeik, K., Kausche,A., Klein, T., Lange, M., Lepland, A., Malnati, J., Meckel, S., Meyer-Schack, B., Noorlander, K., Panieri, G., Pape, T., Reuter, M., Riedel, M., Rosiak, U., Schmidt, Ch., Schmidt, W., Seiter, Ch., Spagnoli, G., Stachowski, A., Stange, N., Wallmann, K., Wintersteller, P., Wunsch, D., Yao, H., 2017. R/V MARIA S. MERIAN Cruise Report MSM57, Gas Hydrate Dynamics at the Continental Margin of Svalbard, Reykjavik – Longyearbyen – Reykjavik, 29 July – 07 September 2016. Berichte, MARUM – Zentrum für Marine Umweltwissenschaften, Fachbereich Geowissenschaften, Universität Bremen, No. 314, 204 pages. Bremen, 2017. ISSN 2195-9633.

Butt, F.A., Elverhøi, A., Solheim, A., Forsberg, C.F., 2000. Deciphering Late Cenozoic development of the western Svalbard Margin from ODP Site 986 results. Marine Geology 169(3), 373–390. https://doi.org/https://doi.org/10.1016/S0025-3227(00)00088-8

Christen, M., Kowalski, J., Bartelt, P., 2010.. RAMMS: numerical simulation of dense snow avalanches in three-dimensional terrain. Cold Reg. Sci. Technol., 1–2, 1–14 (doi: 10.1016/ j.coldregions.2010.04.005)

Dessandier, P.-A., Knies, J., Plaza-Faverola, A., Labrousse, C., Renoult, M., Panieri, G., et al. 2021. Ice-sheet melt drove methane emissions in the Arctic during the last two interglacials. Geology 49. doi: 10.1130/g48580.1Eccleshall, S.V., Hormes, A., Hovland, A., Preusser, F., 2016. Constraining the chronology of Pleistocene glaciations on Svalbard: Kapp Ekholm re-visited. Boreas 45(4), 790–803.

https://doi.org/10.1111/bor.12191

Eccleshall, S. V., Hormes, A., Hovland, A. & Preusser, F. 2016: Constraining the chronology of Pleistocene glaciations on Svalbard: Kapp Ekholm re-visited. Boreas 45, 790–803.

Fiedler, A., Faleide, J.I., 1996. Cenozoic sedimentation along the southwestern Barents Sea margin in relation to uplift and erosion of the shelf. Global and Planetary Change 12(1), 75–93. https://doi.org/https://doi.org/10.1016/0921-8181(95)00013-5

Forsberg, C.F., Solheim, A., Elverhøi, A., Jansen, E., Channell, J.E.T.,Andersen, E.S., 1999, The depositional environment of the western Svalbard margin during the upper Pliocene and the Pleistocene; sedimentary facies changes at Site 986, in Proceedings of the Ocean Drilling Program, Scientific Results, Leg 162, pp. 233–246, edited by M. E. Raymo, E. Jansen, P. Blum, and T. D. Herbert, Ocean Drilling Program, College Station, Texas.

Geissler, W.H., Jokat, W., 2004. A geophysical study of the northern Svalbard continental margin. Geophysical Journal International 158(1), 50–66. https://doi.org/10.1111/j.1365-246X.2004.02315.x

Hampton, M.A. 1972. The role of subaqueous debris flow in generating turbidity currents. Journal of Sedimentary Research 42(4), 775–793. https://doi.org/10.1306/74D7262B-2B21-11D7-8648000102C1865D

Harland, W.B., 1997. Part 1: Chapter 3 Svalbard's geological frame. Geological Society, London, Memoirs 17(1), 23–46. https://doi.org/10.1144/GSL.MEM.1997.017.01.03

Hiscott, R.N., Aksu, A.E., 1994. Submarine Debris Flows and Continental Slope Evolution in Front of Quaternary Ice Sheets, Baffin Bay, Canadian Arctic. AAPG Bulletin 1994; 78 (3): 445–460. doi: https://doi.org/10.1306/BDFF90DC-1718-11D7-8645000102C1865D.

Hjelstuen, B., Eldholm, O., Faleide, J.I., 2007. Recurrent Pleistocene mega-failures on the SW Barents Sea margin. Earth and Planetary Science Letters 258, 605–618. https://doi.org/10.1016/j.epsl.2007.04.025

Hjelstuen, B.O., Elverhøi, A., Faleide, J.I., 1996. Cenozoic erosion and sediment yield in the drainage area of the Storfjorden Fan. Global and Planetary Change 12(1), 95–117. https://doi.org/https://doi.org/10.1016/0921-8181(95)00014-3

Ilstad, T., Elverhøi, A., Issler, D., Marr, J., 2004. Subaqueous debris flow behaviour and its dependence on the sand/clay ratio: A laboratory study using particle tracking. Marine Geology 213, 415–438. https://doi.org/10.1016/j.margeo.2004.10.017

Ingólfsson, Ó., Landvik, J.Y., 2013. The Svalbard-Barents Sea ice-sheet - Historical, current and future perspectives. Quaternary Science Reviews 64, 33–60. https://doi.org/10.1016/j.quascirev.2012.11.034

Jansen, E., Sjøholm, J., 1991. Reconstruction of glaciation over the past 6 Myr from ice-borne deposits in the Norwegian Sea. Nature 349(6310), 600–603. https://doi.org/10.1038/349600a0

Ker, S., Marsset, B., Garziglia, S., Le Gonidec, Y., Gibert, D., Voisset, M., Adamy, J., 2010. High-resolution seismic imaging in deep sea from a joint deep-towed/OBH reflection experiment: Application to a Mass Transport Complex offshore Nigeria. Geophysical Journal International 182(3), 1524–1542. https://doi.org/10.1111/j.1365-246X.2010.04700.x

Ker, S., Le Gonidec, Y., Marsset, B., Westbrook, G.K., Gibert, D., Minshull, T.A., 2014. Fine-scale gas distribution in marine sediments assessed from deep-towed seismic data. Geophysical Journal International 196(3), 1466–1470. https://doi.org/10.1093/gji/ggt497

Laberg, J.S., Vorren, T.O., 1995. Late Weichselian submarine debris flow deposits on the Bear Island Trough Mouth Fan. Marine Geology 127(1), 45–72. https://doi.org/https://doi.org/10.1016/0025-3227(95)00055-4

Laberg, J.S., Vorren, T.O., 1996. The Middle and Late Pleistocence evolution and the Bear Island Trough Mouth Fan. Global and Planetary Change 12(1), 309–330. https://doi.org/https://doi.org/10.1016/0921-8181(95)00026-7

Løtveit, I.F., Fjeldskaar, W., Sydnes, M. 2019. Tilting and Flexural Stresses in Basins Due to Glaciations—An Example from the Barents Sea. Geosciences 9(11). https://doi.org/10.3390/geosciences9110474

Mangerud, J., Dokken, T., Hebbeln, D., Heggen, B., Ingólfsson, O., Landvikn, J.Y., Mejdahl, V., Svendsen, J.I., Vorren, T.O., 1998. Fluctuations of the Svalbard-Barents Sea Ice Sheet During the Last 150 000 Years. Quaternary Science Reviews 17(97), 11–42.

Mangerud, J., Svendsen, J.I., 1992. The last interglacial-glacial period on Spitsbergen, Svalbard. Quaternary Science Reviews 11(6), 633–664. https://doi.org/https://doi.org/10.1016/0277-3791(92)90075-J

Masson, D.G., Howe, J.A., Stoker, M.S., 2002. Bottom-current sediment waves, sediment drifts and contourites in the northern Rockall Trough. Marine Geology 192, 215–237.

Mattingsdal, R., Knies, J., Andreassen, K., Fabian, K., Husum, K., Grøsfjeld, K., De Schepper, S., 2014. A new 6 Myr stratigraphic framework for the Atlantic–Arctic Gateway. Quaternary Science Reviews 92, 170–178. https://doi.org/https://doi.org/10.1016/j.quascirev.2013.08.022

Mohrig, D., Elverhøi, A., Parker, G., 1999. Experiments on the relative mobility of muddy subaqueous and subaerial debris flows, and their capacity to remobilize antecedent deposits. Marine Geology 154(1), 117–129. https://doi.org/https://doi.org/10.1016/S0025-3227(98)00107-8

Mudelsee, M., Stattegger, K., 1997. Exploring the structure of the mid-Pleistocene revolution with advanced methods of time-series analysis. Geologische Rundschau 86(2), 499–511. https://doi.org/10.1007/s005310050157

Mudelsee, M., Raymo, M., 2005. Slow dynamics of the Northern Hemisphere glaciation. Paleoceanography 20. https://doi.org/10.1029/2005PA001153

Myhre, A.M., Thiede, J., Firth, J.V., et al., 1995. Proc. ODP, Initial Reports 151: College Station, TX (Ocean Drilling Program). doi:10.2973/odp.proc.ir.151.1995

Niessen, F., Hong, J.K., Hegewald, A., Matthiessen, J., Stein, R., Kim, H., Kim, S., Jensen, L., Jokat, W., Nam, S.-II., Kang, S.-H., 2013. Repeated Pleistocene glaciation of the East Siberian continental margin, Nature Geoscience 6(10), 842–846, doi:10.1038/ngeo1904.

Ó Cofaigh, C., Taylor, J., Dowdeswell, J.A., Pudsey, C.J., 2003. Palaeo-ice streams, trough mouth fans and high-latitude continental slope sedimentation. Boreas 32, 37–55. doi: 10.1080/03009480310001858

Ritzmann, O., Jokat, W., 2003. Crustal structure of northwestern Svalbard and the adjacent Yermak Plateau: evidence for Oligocene detachment tectonics and non-volcanic breakup. Geophysical Journal International 152(1), 139–159. https://doi.org/10.1046/j.1365-246X.2003.01836.x

Ryseth, A.E., Augustson, J.H., Charnock, M.A., Haugerud, O., Stig-Morten, K., Midbøe, P.S., Opsal, J.G., Sundsbø, G., 2003. Cenozoic stratigraphy and evolution of the Sørvestsnaget Basin, southwestern Barents Sea. Norwegian Journal of Geology 83, 107-130. https://api.semanticscholar.org/CorpusID:166221764

Salm, B., 1993. Flow, flow transition and runout distances of flowing avalanches. Annals of Glaciology 18, 221–226. https://doi.org/10.3189/S0260305500011551

Sarkar, S., Berndt, C., Chabert, A., Masson, D.G., Minshull, T.A., Westbrook, G.K., 2011. Switching of a paleo-ice stream in northwest Svalbard. Quaternary Science Reviews 30(13–14). https://doi.org/10.1016/j.quascirev.2011.03.013

Sarkar, S., Berndt, C., Minshull, T. A., Westbrook, G. K., Klaeschen, D., Masson, D.G., Chabert, A., Thatcher, K. E., 2012. Seismic evidence for shallow gas-escape features associated with a retreating gas hydrate zone offshore west Svalbard. *J. Geophys. Res.*, 117, B09102, doi:10.1029/2011JB009126.

Slubowska-Woldengen, M., Rasmussen, T.L., Koc, N., Klitgaard- Kristensen, D., Nilsen, F., Solheim, A., 2007. Advection of Atlantic Water to the western and northern Svalbard shelf since 17,500 cal yr BP. Quaternary Science Reviews 26, 463–478.

Sobiesiak, M., Kneller, B., Alsop, G., Milana, J., 2018. Styles of basal interaction beneath mass transport deposits. *Marine and Petroleum Geology*, *98*, 629–639. https://doi.org/10.1016/j.marpetgeo.2018.08.028

Solheim, A., Faleide, J.I., Andersen, E.S., Elverhøi, A., Forsberg, C.F., Vanneste, K., Uenzelmann-Neben, G., Channell, J.E.T., 1998. Late cenozoic seismic stratigraphy and glacial geological development of the East Greenland and Svalbard–Barents sea continental margins. Quaternary Science Reviews 17(1), 155–184. https://doi.org/https://doi.org/10.1016/S0277-3791(97)00068-1

Svendsen, J.I., Alexanderson, H., Astakhov, V. I., Demidov, I., Dowdeswell, J., Funder, S., Gataullin, V., Henriksen, M., Hjort, C., Houmark-Nielsen, M., Hubberten, H., Ingolfsson, O., Jakobsson, M., Kjaer, K., Larsen, E., Lokrantz, H., Lunkka, J.P., Lysa, A., Mangerud, J.,Matiouchkov, A., Murray, A., Moller, P., Niessen, F., Nikolskaya, O., Polyak, L., Saarnisto, M., Siegert, C., Siegert, M., Spielhagen, R., Stein, R., 2004. Late Quaternary ice sheet history of northern Eurasia. Quaternary Science Reviews 23, 1229–1271.

Talling, P. J., 2013. Hybrid submarine flows comprising turbidity current and cohesive debris flow: Deposits, theoretical and experimental analyses, and generalized models. Geosphere, 9 (3): 460–488. doi: https://doi.org/10.1130/GES00793.1

Vorren, T.O., Lebesbye, E., Larsen, K.B., 1990. Geometry and genesis of the glacigenic sediments in the southern Barents Sea. In: Dowdeswell, J.A., Scourse, J.D. (Eds.), Glacimarine Environments: Processes and Sediments. The Geological Society Publishing House, Bath, pp. 269–288.

Vorren, T.O., Richardsen, G., Knutsen, S.-M., Henriksen, E., 1991. Cenozoic erosion and sedimentation in the western Barents Sea. Marine and Petroleum Geology 8(3), 317–

340. https://doi.org/https://doi.org/10.1016/0264-8172(91)90086-G

Vorren, T.O., Laberg, J.S., 1997. Trough mouth fans - Palaeoclimate and ice-sheet monitors, Quaternary Science Reviews 16(8), 865-881, doi: 10.1016/S0277-3791(97)00003-6.

Westbrook, G. K., et al., 2009. Escape of methane gas from the seabed along the West Spitsbergen continental margin, Geophys. Res. Lett., 36, L15608, doi:10.1029/2009GL039191.

Wiberg, D.H., Haflidason, H., Laberg, J.S., 2022. An updated Weichselian chronostratigraphic framework of the Kongsfjorden Trough Mouth Fan and its implications for the glacial history of Svalbard. Boreas 51(3), 667–683. https://doi.org/10.1111/bor.12581

Zhao, F., Minshull, T.A., Crocker, A.J., Dowdeswell, J.A., Wu, S., Soryal, S.M.(2017. Pleistocene iceberg dynamics on the west Svalbard margin: Evidence from bathymetric and sub-bottom profiler data. Quaternary Science Reviews 161(1), 30–44. https://doi.org/10.1016/j.quascirev.2017.01.019